PHYSICAL REVIEW B **75**, 214503 (2007)

Self-organized networks and lattice effects in high-temperature superconductors

J. C. Phillips
Department of Physics and Astronomy, Rutgers University, Piscataway, New Jersey 08854-8019, USA

(Received 31 October 2006; published 7 June 2007)

The self-organized dopant percolative filamentary model, entirely orbital in character (no fictive spins), explains quantitatively and uniquely chemical trends in superconductive transition temperatures T_c, assuming that Cooper pairs are formed near soft dopants because there attractive electron-phonon pairing interactions outweigh repulsive Coulomb interactions. According to rules previously used successfully for network glasses, the host networks are marginally stable mechanically. The high T_c's are caused by softening of the host network, enormously enhanced by large electron-phonon interactions at even softer interlayer dopants for states near the Fermi energy. Background inhomogeneities (antiferroelectric pseudogap regions) produce percolative "hydrodynamic" features in phase diagrams. The model is especially successful in describing the appearance of giant magnetic vortex "precursive" effects at temperatures $\sim 2T_c$ far above the superconductive transition temperature T_c. The anomalous precursive temperature-dependent strains observed by extended x-ray-absorption fine structure are associated with relaxation of filamentary ends. *Abrupt* transitions at optimal doping are observed in time-resolved picosecond relaxation spectroscopy at 1.5 eV, and these are explained as well using no new assumptions and no adjustable parameters. The theory *resolves* the mystery of the vanishing isotope effect at optimal doping. Both broad and detailed features of global atomic-scale tunneling characteristics reported in 2007 in underdoped cuprates are in excellent agreement with the lateral and/or vertical zigzag filamentary model discussed in 1990.

DOI: 10.1103/PhysRevB.75.214503 PACS number(s): 74.72.−h

I. INTRODUCTION

High-temperature cuprate superconductivity may be the most complex phenomenon known in inorganic materials. It has been the subject of more than 65 000 papers, and a large number of theoretical models have attempted to explain the many counterintuitive phenomena observed. Many of the theoretical papers contain elaborate and ingenious many-body spin models whose relation to experiment is tenuous. In this paper, hierarchical topological methods, based on the author's earlier theories of the glassy behavior of dopants in the cuprates,[1] are used to discuss several anomalies in detail, with emphasis on the key role played by the connectivity of the internal dopant structure. The theory emphasizes qualitative trends, as experience has shown that the complexity of these materials may well preclude quantitative treatments of the kind that worked so well for simpler superconductors, such as MgB_2.[2] The theory aims to combine quite general mathematical principles with a close analysis of experimental results, while it emphasizes not general many-body, but highly material-specific, mechanisms—after all, high-temperature superconductivity (HTSC) is a unique phenomenon.

Scanning tunneling microscopy (STM) has revealed a strongly disordered, patchy (~ 3 nm) pattern of gap inhomogeneities in nearly optimally doped $Bi_2Sr_2CaCu_2O_{8+x}$ (BSCCO),[3–5] with patterns strongly dependent on the concentration x of interstitial oxygen dopants O_x. These patterns are the result of projecting three-dimensional structure onto a two-dimensional field of view, which still leaves many aspects of the true three-dimensional structure unknown. Continuum methods (including Fourier transforms) explain only a very small part of these two-dimensional patterns, with the remainder being left as mysterious "dark matter." The dopant network model explains many more aspects, all within a unified framework; its central features have recently been confirmed by STM (see the Appendix). The complex, partially hidden and strongly disordered structure of the cuprates appears to be essential to their unparalleled properties as high-temperature superconductors: for example, the development of superlattice ordering at commensurate doping concentrations [the 1/8 "stripe" phase of $La_{2-x}Sr_xCuO_4$ (LSCO)] greatly reduces T_c, probably to zero when fully developed. Experience with exponentially complex molecular and network glasses has shown that no single polynomial mechanism describable by mean-field theory can provide a satisfactory explanation for such optimal properties; instead, one attempts to identify multiple factors, *all* of which are optimized. Meanwhile, "rigorous" formal polynomial lattice models leave the question of the microscopic mechanisms responsible for the gaps, their inhomogeneities, and the origin of HTSC itself, and even the origin of the HTSC intermediate phase,[1] open.

Many readers have found the topological approach described here to be too abstract: they long for some kind of simple analytic model that contains adjustable parameters that can be fitted to experiment. There is an interesting historical precedent for the shift from easily parametrized analytic models to topological models. After Newton solved the problem of planetary motion (essentially a one-body problem in the central field approximation), D'Alembert addressed the hydrodynamic problem of fluid motion. From the Newtonian viewpoint, this is a hopelessly complex many-body problem, and even today no exact analytic solutions are known for the general problem of fluid motion subject to general boundary conditions. However, everyone knows that this motion exhibits general properties (turbulent and nonturbulent flows, streaming, eddies, growth rates of unstable modes, etc.). The analysis of these properties has evolved over the past 300 years (not an easy problem, in fact, attempts to oversimplify hydrodynamic equations to make them look homogeneous are still being criticized[1]), and topological methods have played a crucial role in that analysis. Conversely, historians say that the calculus of variations originated with D'Alembert's interesting hydrodynamics. This, in turn, led to the development of Lagrangian mechanics, which contains both analytic and topological elements. The Lagrangian methods involve (topological) paths in configuration space whose properties are constrained by variational principles. Even in vacuum, the Lagrangian path approach is useful (Feynman path integrals, for example), but it is much more useful in strongly disordered cases where only large-scale features of the internal atomic structure are known.

Readers who still find this description too abstract should recall three classic problems in mechanics: the disk rolling down an inclined plane without slipping, Huygens' tautochrome (a pendulum whose frequency is independent of amplitude), and Bernoulli's brachistochrome, the curved path between two points with the shortest transit time subject to a constant vertical force. These three (apparently different) problems all share a common solution (the cycloid), because they contain common variational features and involve similarly constrained combinations of lateral and vertical motions. In fact, the optimized dopant-centered zigzag current paths in the cuprates all exhibit similar special properties because they also combine constrained two-dimensional lateral and three-dimensional (lateral+vertical) motions.

Only a few theories have attempted to describe HTSC in the cuprates starting from a strongly disordered model with characteristics intermediate between those of ideal crystals and an array of large and overlapping nanodomain "molecules" containing thousands of off-lattice atoms. Although different in many details, the "negative U" model discussed by Wilson[6] comes closest to the present one in emphasizing the importance of soft lattices and ultrastrong electron-phonon interactions at dopants. The present model goes further than negative U models; however, in several critical respects, notably, U is a "hidden" variable. Although U surely varies from cuprate to cuprate and eventually determines observables such as T_c, we will see that there are many universal features of the cuprates that are hierarchical and topological in nature and do not depend explicitly on the value of U.

II. SIMPLE (YET PARADOXICAL) EXAMPLE

The superconductive energy gap Δ plays a key role in all microscopic theories, starting with the simple metallic "low-temperature" superconductors such as Al, Sn, and Pb.[7] It is caused by the formation of Cooper pairs, combined in the BCS product many-pair wave function. The gap occurs because the attractive electron-phonon interactions exceed the repulsive Coulomb interaction in the s-wave ($l=0$) channel. In superfluid ^{3}He, the $l=0$ s-wave interaction is repulsive, but the residual $l=1$ p-wave interaction is weakly attractive, leading to superfluidity at a much lower temperature than in ^{4}He. By this reasoning, the appearance of $l=2$ d-wave anisotropy (with little or no $l=0$ term) in the energy gap of the cuprates (in early surface measurements of relative grain-boundary phases,[8] ARPES,[9] or Fourier-transformed STM gap patterns[10]) would be consistent only with ultralow T_c's, so there is a major puzzle here. One way to resolve this puzzle is to note that the d-wave pattern can be strongly enhanced at the surface and much smaller in the bulk ("d outside and s inside").[11] However, there is a similar, but more fundamental reason, why the d-wave symmetry (which also appears in the pseudogap[12]) is incidental to the microscopic mechanism responsible for HTSC.

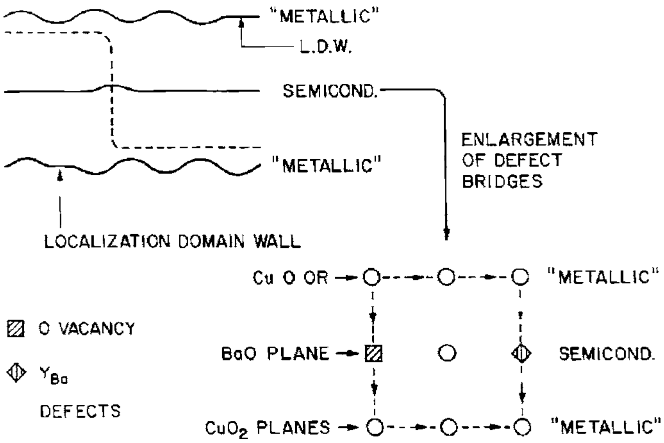

FIG. 1. The basic idea of the filamentary paths in the quantum percolative model (Ref. 14) for YBCO. The positions of the insulating nanodomain wall (INW pseudogaps) in the CuO$_2$ layers are indicated, together with the resonating tunneling centers (RTC dopants) in the semiconductive layer and oxygen vacancies in the CuO$_{1-x}$ chains. Giant e-p interactions are associated with the RTC, where the interactions with LO c-axis phonons are especially large. The INWs are perovskite specific. The *sharp bends* in the filamentary paths are responsible for the broken symmetry that admixes ab planar background currents with c-axis LO phonons. The interrupted filamentary surface morphology implied by this figure from 1990 has recently been observed in underdoped samples by STM (Ref. 91), using instrumentation reported from 2002 and after Ref. 5.

The filamentary network model[1] resolves the s-d puzzle in a simple way, which is consistent with the large bulk energy gaps and high T_c's extending up to and including the last surface layer seen in STM experiments. The d-wave anisotropy is exhibited only in the (two-dimensional) xy plane; using z as the polar axis, this corresponds to an $l=2$, $m=2$ spherical harmonic. However, according to the filamentary model [see Fig. 1, which dates back to 1989 (Ref. 1)], the strong s-wave ($l=m=0$) atomic-scale electron-phonon interactions occur at the negative U interlayer dopants (often interstitial O) that connect partially conductive layers. At these dopants, the three-dimensional (lateral and/or vertical) path is parallel to the z axis, and the strong s-wave electron-phonon interactions at the interlayer dopants have no effect on the phase coherence of paths projected on the xy plane. There the topologically constrained superconductive paths follow the directions of largest electron wave-packet group velocities and strongest local electron-phonon interactions between metal atoms and O atoms, where the longitudinal-

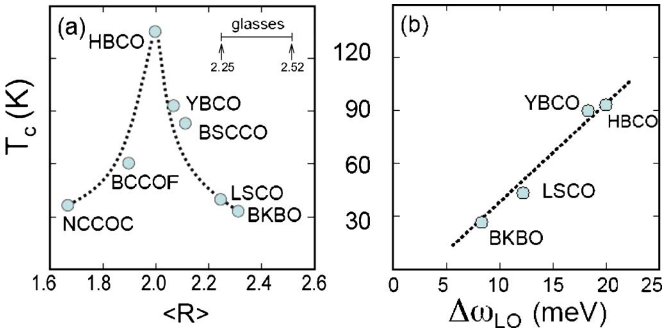

FIG. 2. (Color online) (a) Chemical trends in $T_c^{\max}$ with $\langle R\rangle = \langle |Z| \rangle$, which measures the global stiffness of the doped crystalline network, with $Z(\mathrm{Cu})=2$, $Z(\mathrm{Bi})=3$ (4) [BSCCO ($Ba_{1-x}K_xBiO_3$, BKBO), as in the parent insulators, where $\Sigma Z=0$], and $Z(\mathrm{O})=-2$. Perovskites ($R=2.40$) and pseudoperovskites are only marginally stable mechanically (Ref. 20), and for HTSC cuprates, $\langle R\rangle$ lies in the region of floppy networks just below the isostatic (rigid but unstressed) range determined by studies of network glasses (brackets). The peak in $T_c^{\max}$ occurs at $\langle R\rangle=2$, as one would expect from mean-field percolation theory. The point for BCCOF was added after the figure was drawn originally, and the original curve has not been modified. (b) The cuprates are stabilized by antiferroelectric checkerboard reconstruction, the strength of which may determine the $\Delta\omega_{LO}$ phonon (half-breathing mode) anomaly, which also correlates well with T_c. (The single crystal sample[32] of Hg1201 had $T_c=94$ K.) Dashed lines are guides only. NCCOC, $Na_xCa_{2-x-y}CuO_2Cl_2$; BCCOF, $Ba_2Ca_3Cu_4O_8F_2$; HBCO, $HgBa_2Ca_2Cu_3O_8$; YBCO, $YBa_2Cu_3O_{6+x}$; BSCCO, $Bi_2Sr_2CaCu_2O_{8+x}$; LSCO, $La_{2-x}Sr_xCuO_4$ and La_2CuO_{4+x}; BSCO, $Bi_2Sr_2CuO_{6+x}$.

optic (LO) phonons show strong (10) zone-boundary anomalies [Fig. 2(b)]. Thus, because the paths are not indexed by crystal momentum, but rather by sets of nearest-neighbor vectors in real space, they appear to have *d*-wave symmetry in the *xy* plane, while actually representing Cooper pairs formed by *s*-wave interactions at the dopants. The planar *d*-wave symmetry is incidental and is merely the consequence of projecting the three-dimensional (xy,z) zigzag paths in real space onto two-dimensional *xy* planar Fourier transforms. Note that these two-dimensional paths must still percolate through a planar pseudogap maze that has largely *d*-wave *x*-*y* symmetry, as the antiferroelectric (zone-boundary) LO phonon itself has *d*-wave symmetry. One technical comment is that the *s*-wave interactions occur on the atomic scale[6] and, technically speaking, represent a very large local-field correction to the interactions forming Cooper pairs. In the filamentary model, they are hidden from and do not appear in the *x*-*y* planar angular Δ, because of their orthogonal (vertical) out-of-plane *z*-axis character.

III. ELEMENTS OF THE TOPOLOGICAL MODEL

The modern theory of glasses is called constraint theory;[1] it accurately describes the phase diagrams of both molecular glasses (window glass) and electronic glasses (the cuprates). (The theory identifies self-consistent network properties, and this accounts for its generic success.) In the molecular case (network glasses such as window glass), the constraints are counted by analyzing interatomic bonding forces (stretching bending, etc.). The mean-field condition for forming an ideal glass is $N_c=N_d$, where N_c is the number of constraints per atom and N_d is the number of degrees of freedom per atom. In a gas of N atoms, $N_d=2d$ (position and momentum), but in a glass $N_d=d$, as the glass is frozen into a configuration of nearly maximal density (ideal space filling for a strongly disordered network), with only spatial degrees of freedom (periodic crystalline configurations are, of course, singular and not glassy). Cuprates are electronic glasses, with the dopants frozen into configurations that minimize the free energy by nearly optimally screening internal electric fields. Constraint theory is topological, not analytical, and it is capable of describing such variational effects by Lagrangian methods without detailed knowledge of glassy configurations, in both molecular (window glass) and electronic (cuprate) glasses. Analytical models of continuum systems have been able to derive results not only for simple nearly-free-electron metals but also even for weakly disordered metals (dirty transition metals, etc.). They are, however, completely unsuited to strongly disordered, nanoscopically inhomogeneous ceramic metals with anomalous properties obtained by adaptively doping an insulator, such as the cuprate high-temperature superconductors.[3–5]

While there are many crystalline materials, there are only a few ideal glass formers. These, in turn, have properties that are very, very different from those of normal materials, and these properties are often of great value, which has focused attention on them. Constraint theory correspondingly is of little value in discussing most materials, because the ideal glass-forming condition $N_c=N_d$ is seldom satisfied. However, when circumstances make it possible to form ideal glasses, constraint theory is very powerful.[1] It is able to explain, without using adjustable parameters, why cuprates [and to a lesser extent the cubic perovskite (Ba,K)(Pb, Bi)O_3 family] are the only materials that form high-temperature superconductors,[12] a highly material-specific result inaccessible to analytic theories, even with the customary adjustable parameters.

Figure 1 illustrates the basic topological model for layered cuprate high-temperature superconductors. Semiconductive layers (such as SrO) alternate with metallic layers (CuO_2, BiO). The planar lattice constant is fixed by the isostatically (stress-free) rigid CuO_2 layers, which stabilize the structure mechanically and satisfy the ideal glass-forming (space-filling network) condition $N_c=N_d$ with regard to interatomic forces.[11] The remaining layers are much softer (or floppier) and are easily distorted: this explains why the only electronic states near E_F that are observable by ARPES are those associated with CuO_2 layers. It is customary to assume that the CuO_2 layers are perfectly crystalline, but because of the interlayer misfit to semiconductive layers (such as SrO) of effectively different relaxed lattice constants, this is almost certainly not the case.[1,12,13] The misfit can be relieved, and the total energy reduced, by inserting thin (semi-)insulating domain walls in the CuO_2 layers. Because the Cu $d(x^2\text{-}y^2)$-O $p(x,y)$ conduction band is nearly half full, the natural choice for such walls would be multiple antiferroelectrically doubled unit cells, Jahn-Teller distorted in such a way as to introduce a small anisotropic energy pseudogap (or depression in the local density of states), analogous to that formed by a charge-density wave. Because of the overall softness of the lattice, the gain in electronic energy from forming such a pseudogap is reduced only partially by the increased elastic strain energy. Projected onto a surface plane and observed by STM, these pseudogaps are part of the irregular gap structure observed by STM, and in optimally doped samples,[5] the two gaps are not easily separated. They have been separated recently in underdoped samples (see the Appendix).

The splitting of the metallic CuO_2 planes into nanodomains separated by insulating domain walls results in a narrow gap semiconductor. Now, as the x dopants are added, usually to the alternating semiconductive layers (such as SrO), they provide negative U (Ref. 6) bridges that can carry current in zigzag paths around the domain walls (Fig. 1). (In fact, in this case, the disordered domain walls that make the CuO_2 planes semiconductive in isolation actually make HTSC possible, because they force the current paths to pass through the soft negative U dopants where the electron-phonon interactions are very strong. Of course, this scenario is very unlikely, but so is HTSC: if the shoe fits, wear it.) These paths form dopant-centered conducting wires, and there is an insulator-metal transition when there are enough dopants that the wires begin to percolate at $x=x_1$. This *percolative* metallic phase is qualitatively different from a quasi-one-dimensional normal metal with weak localization, because the filamentary density increases with x. At $x=x_0$, it reaches a maximum (space is filled), and at larger values of x, the filaments bunch together so closely that interfilament scattering converts the bunched regions into regions that are locally normal metals.[14] In these normally metallic regions, the local density of states near E_F is much larger than when averaged over the filaments and semiconductive background. These zigzag paths are a useful tool for analyzing the relation between anomalies in LO phonon spectra measured by neutron scattering.[14] They also provide a derivation[14] of the d-wave gap by projection of the paths on preferred antinodal directions; in this microscopic model, nodal gap quasiparticles are replaced by *projections* of Cooper pairs bound to independent filaments onto nodal (π,π) gap directions. These are the directions along which percolation between nanodomains with edges parallel to Cartesian directions is most effective in dielectric screening.

A more formal description of the origin of the zigzag paths proceeds as follows. For simplicity, we assume that all the negative U (Ref. 6) dopant bridges are locally equivalent. [This is a good approximation because the domain walls are similar; they relieve the global interlayer misfit. Similarly, the negative U dopants are similar, because they adopt the optimal bridging positions that maximize the dopant-assisted tunneling through (or around) the dopant walls.] In a mean-field approximation, the coherence of the dopant impurity band network is now measured by the structure factor $S(\mathbf{k}) = \Sigma_i \exp(i\mathbf{k}\cdot\mathbf{r}_i)$, where the sum extends over all dopant sites $\mathbf{r}_i$. Such a sum, in the presence of many-electron thermal fluctuations, rapidly becomes incoherent. However, if we separate the sum into its filamentary components f as a double sum $S(\mathbf{k}) = \Sigma_f \Sigma_i \exp(i\mathbf{k}\cdot\mathbf{r}_{if}) = \Sigma_f S_f(\mathbf{k})$, then each filament f contains only a few electrons, so that the average interlevel energy spacing on a given filament (now of order $N^{-1/3}$ instead of N^{-1}) becomes large compared to kT. Thus, the filaments are separately coherent or incoherent (each filament has its own phase or order parameter). In the absence of filamentary overlap, the internal coherence of the "intact" filaments is affected only marginally by interfilamentary interactions with the incoherent filaments.

Before we leave this topic, it is important to ask whether or not these interlayer zigzag paths can be described in terms of interlayer Josephson coupling. The short answer is no. The tunneling Hamiltonian[15] that describes the Josephson effect associated with tunneling through an oxide barrier between two metals assumes that superconductivity is strong in the metals and that the tunneling interaction energy $\mathcal{J}$ (averaged laterally over the barrier) is weak and can be treated perturbatively. In the cuprates, the carrier density in the CuO_2 planes is low (one carrier per large unit cell), and in such cases, the electron-electron Coulomb repulsion is generally larger than the electron-phonon attraction—in other words, the CuO_2 planes alone are probably not even superconductive. It is the strongly attractive electron-phonon pairing interactions at the interlayer dopants that causes HTSC, and these cannot be treated perturbatively. This is why it is essential to introduce self-organized zigzag percolative paths into the theory at the outset to describe combined lateral-vertical wavelet motion.

IV. SOFT HOST LATTICES AND CHEMICAL TRENDS IN $T_c^{\max}$

In the older metallic and intermetallic superconductors, there were many correlations between lattice softening and higher T_c's (for instance, the Al lattice is hard, Sn is softer, and Pb softer still, and the T_c's increase correspondingly). The reason for this trend is that stronger electron-phonon interactions mean better electron-ion dielectric screening of ion-ion repulsion.[7] Are there any corresponding trends in T_c or $T_c^{\max}$ (the largest value of T_c for a given alloy family at $P=0$) in the cuprates?

There are. Uemura[16] connected T_c and n_s, where n_s is estimated from magnetic-field penetration depths λ measured by muon spin relaxation. The data show that T_c is nearly linear in n_s for many cuprates, including samples with T_c depressed by Zn doping in CuO_2 planes. Within the filamentary model, optimized T_c's ($T_c^{\max}$) can be estimated by scaling filamentary spacings as follows. Each filament, with the dopants arranged like pearls on a string, binds its own set of dopant-derived one-electron states that are phase correlated to produce maximum conductivity, and hence maximum screening of fluctuating internal ionic fields, with the dopants occupying optimized curvilinear threading positions during sample annealing, and refining these positions with decreasing temperature. Below $T_c^{\max}$, the fraction of filaments with mutually correlated phases is proportional to $n_s(T)/n_s(0)$. At $T=T_c^{\max}$, Cooper pair phase coherence is erased by phase-disruptive interfilamentary phonon absorption. The average spacing between planar filaments (or by three-dimensional filaments projected onto metallic planes) is d, and $dn_s \sim 1$.

Thus, as n_s decreases, the spacing between paired filaments increases, and $T_c^{\max}$ decreases with the absorbed phonon energy.

We now look for the phonon that will be most effective in displacing paired filaments from their optimal configuration. The filaments zigzag from soft gray dopants outside CuO_2 planes (where electron-phonon interactions are large and Δ_s is large locally) through paths in hard black CuO_2 planes (where Δ_s is small and probably would be 0 except for proximity effects) to the next soft gray dopant. The parts of the filamentary path most easily disrupted are therefore the weak links in the CuO_2 planes, which are common to all the cuprates, and the phonon we are looking for belongs to these planes. Because the CuO_2 planes are the stiffest and least disordered element in the host lattice, the dispersion of these phonons is easily measured:[17] the maximum energy at the (100) longitudinal-acoustic phonon at the zone boundary is $\omega_0 = 10$ meV. The actual energy of the phase-breaking phonon should be of order $T_c^{\max}$. Combining these equations, one finds $T_c^{\max} \sim p n_s(0)$. Thus, (100) LA phonons set the overall energy scale for HTSC. The proportionality factor p is not easily estimated, as so little is known about filamentary geometry, but it is approximately independent of doping.

There is an important feature of HTSC phase diagrams that is easily understood from Fig. 1. In order for currents to be forced through the interlayer dopants, the condition $\Delta_p - \Delta_s > 0$ must be satisfied. With $z = x/x_0$, for small z, both $T_c(z)$ and $T_p(z)$ are, respectively, linearly increasing (decreasing) with increasing z, but they cannot cross. The "noncrossing" condition $\Delta_p - \Delta_s > 0$ makes $T_c(z)$ flatten and appear to be quadratic while $T_p(z)$ remains linear as z increases to 1. On the overdoped side, the filaments overlap to form Fermi-liquid patches[14] whose area increases as z increases above 1. We can safely assume that p is larger than in conventional superconductors because filamentary (one-dimensional) glassy topology takes advantage of self-organization to be more efficient in constructing high-conductivity vortex loops to expel or screen magnetic fields than (three-dimensional) electron gases (Sec. X).

The complexity of strong glassy disorder generally prevents the successful construction of polynomial models of glasses. In their place, one usually finds several trends: these trends reflect the combined effects of optimization of properties of most interest, which in HTSC has consisted largely of maximizing T_c (although other properties are also likely to be important for applications). There is another trend apart from the Uemura correlation, referring to variations in $T_c^{\max}$ with host-lattice properties. This trend is connected with host-lattice instabilities and softening; these are characteristic features of strong electron-phonon coupling and have already been observed to limit $T_c^{\max}$ in alloys of the old intermetallic superconductors involving (for example) NbN and Nb_3Sn.[18]

First-principles calculations of T_c based on electron-phonon interactions (EPI) in self-consistent electronic structures with ideal atomic positions are usually quite accurate for "old" superconductors [such as MgB_2 (Ref. 2)], but such calculations for cuprates yield T_c's too small by factors of ~ 100.[19] This failure indicates the breakdown either of conventional EPI or of the ideal lattice structure, leading to enormously enhanced interactions due to the glassy character of negative U (Ref. 6) dopant configurations; experiment has amply demonstrated that the latter are present, as they violently disturb ideal cuprate vibrational spectra,[14] introducing localized vibrational modes into the valleys of the phonon density of states of the parent insulator. Conventional lattice dynamics (even empirical spring constant models) encounters many technical difficulties in the cuprates. Not only is the number of atoms per unit cell large, but also the basic structural unit is actually a nanodomain containing $\sim 10^3$ vibrational degrees of freedom. Thus, statistical methods become important, and because of optimized dopant disorder (exponentially complex broken symmetry), the relevant statistics are those of glasses, not gases, liquids, or crystals. The cuprates are closely related to perovskites (such as $BaTiO_3$), many of which are (anti)ferroelectrics, and nearly all of which are marginally stable elastically and strongly disordered, with nanodomains similar to the cuprates (for instance, manganite perovskites[20]).

Lattice softening can be calibrated by treating cuprates and perovskites as incipient glasses, subject to axiomatic rigidity rules similar to those of network glasses.[1] It is important to realize that these rules have been tested exhaustively, over the past 25 years, against a very large database derived from commercially very successful materials. These rules are simplest and most easily justified for chalcogenide glass alloys composed of atoms of similar size,[21] but more general rules have succeeded for oxide glasses, notably window glass,[22] which is 74% SiO_2 alloyed with 16% Na_2O and 10% CaO. These chemical proportions of window glass, an ideal, globally and locally stress-free network, are partially explained in terms of the average number $\langle R \rangle$ of Pauling resonating valence bonds and/or atom, with $\langle R \rangle = 2.40$ *exactly* [$R = |Z|$, $Z(\mathrm{Na}) = 1$, $Z(\mathrm{Ca}) = 2$, $Z(\mathrm{Si}) = 4$, and $Z(\mathrm{O}) = -2$]. The results[21] for the Boolchand intermediate phase of many ideally stress-free binary and ternary chalcogenide alloy network glasses range from $\langle R \rangle = 2.27$ to $\langle R \rangle = 2.52$; the entire set of ranges is centered on the "magic number" $\langle R \rangle = 2.40$.

Given this background, is there a way to understand both ferroelectrics and cuprates? There is. $\langle R \rangle$ of many ferroelectric perovskites (such as $BaTiO_3$) is 2.40; these perovskites have large energy gaps, and they can be alloyed with isovalent elements (for example, the commercial ferroelectric $[\mathrm{Pb,Zr}]\mathrm{TiO}_3$), but not doped, and they are noted not only for their ferroelectric properties but also for their lattice instabilities and ferroelasticity. With decreasing $\langle R \rangle$, lattices soften, and we reach the dopably metallic HTSC cuprates. Here, we must be careful as the values of R can be ambiguous for polyvalent elements such as Cu and Bi. We can determine R for these elements by demanding that $\Sigma Z = 0$ for the parent insulator. Thus, the parent compound of $La_{2-x}Sr_xCuO_4$ (LSCO) is La_2CuO_4, and with $Z(\mathrm{La}) = +3$ and $Z(\mathrm{Cu}) = +2$. With $Z(\mathrm{Cu}) = +2$, the remaining values of Z are easily determined. For instance, in $Bi_2Sr_2CaCu_2O_8$ (BSCCO), $Z(\mathrm{Sr}) = Z(\mathrm{Ca}) = +2$ and $Z(\mathrm{Bi}) = +3$. On the other hand, in the cubic perovskite $BaBiO_3$, $Z(\mathrm{Bi}) = +4$ (in the language of resonating chemical bonds, Bi has mixed valence: one Bi has $Z = +3$ while the other has $Z = +5$). One can easily calculate $\langle R\rangle$: for example, $\langle R\rangle(\mathrm{La_2CuO_4})=(2.3+2+4.2)/(2+1+4)=16/7$ and $\langle R\rangle(\mathrm{BSCCO})=32/15$. The results for $T_c^{\max}$ in the cuprates are plotted in Fig. 2(a) for $\langle R\rangle$ values corresponding to optimal doping, but if they are replaced by the $\langle R\rangle$ values for the parent insulator (zero doping), the curves would change little. This is because doping typically changes $\langle R\rangle$ by 1%, while there are uncertainties in $T_c^{\max}$ of order 10 K (10%) due to factors other than $\langle R\rangle$ (chiefly the number of $\mathrm{CuO_2}$ planes per unit cell). We find $\langle R\rangle$ values at optimal doping which span the range from $\langle R\rangle=1.67$ up to 2.24 [Fig. 2(a)], which lies just below the edge of the range [2.27, 2.52] of stress-free network glasses.

Note that $T_c^{\max}$ itself reaches its maximum value at $\langle R\rangle=2.0$ ($T_c=135$ K). In fact, the resonance character of $T_c^{\max}$ can be represented by the function $T_c^{\max}(\langle R\rangle)=\Theta f(\langle R\rangle)/f(2)$, with $f(\langle R\rangle)=\exp(-b|\langle R\rangle-2|/W)$, with $W=0.25$, $\Theta=135$ K, and $b=1.2$. Here, the scale factor Θ in some sense reflects the *variable* negative U interactions[6] at the (usually interlayer interstitial O) dopants, yet it is a *constant* for all optimized cuprates, in spite of considerable differences in chemistry and structure. The most significant chemical trends are actually contained in $\langle R\rangle$, which reflects the global softness of the host network (doped or undoped). Microscopic cuprate properties can change qualitatively at $\langle R\rangle=2$. Clearly the superconductive interactions are adaptive, and when superconductivity is optimized, the effective value of U (an *adjustable parameter*, never measured) is represented by the constant Θ.

Note that the progression of the cuprates from larger to smaller values of $\langle R\rangle$ is also that of the chronological order in which good single-crystal samples became available (BKBO, LSCO, YBCO, BSCCO, HBCO, and the $\langle R\rangle<2$ Cl and F materials). This explains why the cuprates are so special: as $\langle R\rangle$ decreases and the host network softens, growing good crystals becomes more difficult for $\langle R\rangle<2.40$ (the perovskite value), and the difficulty increases with decreasing $\langle R\rangle$. This result and all the results shown in Fig. 2(a) are well outside the reach of any analytical model based merely on a polynomial Hamiltonian, where all the global chemical trends are buried in adjustable parameters.

There is an easy way to see why $T_c^{\max}$ reaches its maximum value at $\langle R\rangle=2.0$. To stabilize the structure (assumed to be glassily disordered on a nanosecond time scale, although largely periodic, except near dopants, when averaged over laboratory times) and at the same time maximize softness, each atom should be optimally connected to its two closest neighbors. This requires two resonating bonds: the classic example is an $s+p_x$ hybrid oriented along the x axis, but any two atomic orbitals can be combined to give directionality. The $s+p_x$ hybrid optimally connects an atom at the ($x=0$, $y=0$) origin to atoms at $(-(a\pm\delta),\pm\varepsilon)$ and $(a\pm\delta,\pm\varepsilon)$. This noncrystalline molecular construction can be generalized to any pair of noncolinear (zigzag) nearest-neighbor configurations. Another way of seeing that $\langle R\rangle=2$ is optimal is to note that Cl ($R=1$) forms diatomic molecules, while Se ($R=2$) forms spiral (space-filling) chains. Of course, the most striking fact is that all the atoms apparently contribute with equal weights in maximizing $T_c(\langle R\rangle)$ across the entire master curve. This is a true networking effect: moving any one atom, even an atom far removed from the $\mathrm{CuO_2}$ planes, affects all the other atoms, and the degrees of freedom associated with atoms even in insulating layers are utilized with perfect efficiency in organizing the network to maximize $T_c(\langle R\rangle)$.

In the range $\langle R\rangle<2.40=\langle R\rangle$ (perovskite, for example, ferroelectric $\mathrm{BaTiO_3}$), oxide crystalline networks are anomalously soft, and one would have expected *a priori* that any metallic states at the Fermi energy should be erased by Jahn-Teller distortions, in the cuprates specifically by buckling of the tetragonal basal planes. Experimentally, it has been observed that such buckling (octahedral rocking) is incipient and does limit T_c, but the distortions are small because of the isostatic (rigid but unstressed) nature of the $\mathrm{CuO_2}$ planes.[12] Thus, these rigid planes are not the "glue" or the site of the strong interactions which produce HTSC. Quite the opposite, those interactions occur at the negative U (Ref. 6) dopants in soft planes (the true glue) outside the $\mathrm{CuO_2}$ planes, while the $\mathrm{CuO_2}$ planes function in two other ways: (1) as mechanical stabilizers against Jahn-Teller distortions and (2) as highly conductive media through which Cooper pairs formed by strong electron-phonon interactions at interlayer dopants can connect through S(dopant)-N($\mathrm{CuO_2}$ plane)-S(dopant) (super-norm-super) tunneling. Note, by the way, that the oxichloride, $\mathrm{Na_xCa_{2-x-y}CuO_2Cl_2}$ [NCCOC, $T_c(x=0.2,y=0)=28$ K, $\langle R(0.2,0)\rangle=1.67$], forms a poor network [because $R(\mathrm{Cl})=1$], but with the assistance of Na to bridge the $\mathrm{CuO_2}$ planes, self-organization, and stabilization by a 4×4 antiferroelectric charge-density wave (CDW) checkerboard,[23] it still manages to be superconductive. Replacement of Na by Ca vacancies increases $\langle R\rangle$, reduces defects, and gives $T_c(x=0,y=0.2)=38$ K.[24] Finally, although polaronic effects are strong in all the cuprates,[25] they are especially strong in $\mathrm{Na_xCa_{2-x-y}CuO_2Cl_2}$ because two ions (Na and Cl) have $R=1$.

Perhaps the strongest argument against electron-phonon interactions as the source of HTSC has been the disappearance of the oxygen isotope shift in T_c, which is large and normal near the metal-insulator transition (MIT) but decreases toward a small (but still nonzero) value near $z=1$.[26,27] The variational nature of flexible self-organized percolation explains this long-standing mystery. As discussed more quantitatively in Sec. XIII, near the MIT, the paths are far apart and isotopic substitution does not alter the phonon dynamics that causes the normal isotope shift. However, at $z=x/x_0=1$, the dynamic effects are compensated by the combined effects of zero-point vibrations[18] and space filling. Site-selective isotope shifts in the host lattice[26] are an acid test for this explanation. The $\mathrm{CuO_2}$ planes are isostatic[12] and nearly ideally crystalline and, hence, exhibit an O isotope effect, but the low R planes between them (such as BaO, $R=2$) are soft and glassy, so there is no isotope effect at the apical oxygens or the $\mathrm{CuO_x}$ chains. Thus, there is only a small isotope effect on T_c at optimal doping, even though a normal (3 meV) isotope effect is observed by ARPES for the states between E_F and $E_F+\theta_D$.[28]

A third factor involving soft lattices is the local topology associated with the (100) longitudinal-optic (LO) phonon kinks;[14,29] these occur near $\mathbf{G}/4=(1/2,0,0)$ and may be related to the 4×4 checkerboard pattern that appears to be associated with pseudogaps in underdoped patches.[4] (In insulators, these instabilities are associated with antiferroelectric phases.[30]) Probably, the most instructive data on the LO phonon anomaly are those[29] taken for YBCO at light doping ($x=0.2$) below the MIT, at the MIT ($x=0.35$), in the 60 K plateau ($x=0.6$), and at optimal doping ($x=0.92$). Before long CuO chains have formed ($x=0.2$), only strong and broad LO scattering (labeled N_2) occurs near $\mathbf{q}=(q\ 0\ 0)$ with $q=3.0$ at 73 meV, reflecting the strong disorder and the validity of mean-field models. As soon as the CuO chains percolate ($x=0.35$), a new LO band (labeled Z_3) appears near the zone boundary ($q=3.5$) at 57 meV. When the minor cross-linking chains have begun to percolate ($x=0.6$), both N_2 and Z_3 broaden, and the gap $\Delta\omega_{\mathrm{LO}}$ near $q=3.25$ increases, indicating phase separation between the nanodomains[7] with and without minor chains. At optimal doping ($x=0.92$), there is only one phase, but it is ideally glassy,[8] and the mean-field component N_2 has become very weak while the percolative component Z_3 is very strong.

Z_3 is the "half-breathing" mode seen in all the cuprates and is often described as an intrinsic property of the $\mathrm{CuO_2}$ planes.[2] However, in YBCO, where the doping dependence is best known,[14,29] it appears that the buckling, although observed in the $\mathrm{CuO_2}$ planes, is induced by the CuO chains, and not (for example) by large positive U's at the Cu atoms of the $\mathrm{CuO_2}$ planes.[2] In other words, the instability is caused by the marginal elastic stability of the entire network, including chains, planes, and the intervening soft insulating layers.

As all factors must conspire variationally to produce HTSC, one can assume that the LO phonon gap $\Delta\omega_{\mathrm{LO}}$ is one of them and plot $T_c^{\max}$ against $\Delta\omega_{\mathrm{LO}}$ [Fig. 2(b)]: again, there is a strong correlation. Considering that $T_c^{\max}$ is limited by T_p and that the pseudogap phase is apparently stabilized by the 4×4 checkerboard pattern associated with it, this correlation is natural. Of course, space filling produces the sharpest LO phonon gap, which occurs at optimal doping ($T_c=T_c^{\max}$) in $\mathrm{La_{2-x}Sr_xCuO_4}$ (LSCO), $x=0.15$; this gap is just as sharp as in the $x=1/8$ crystalline stripe phase,[32] where $T_c=0$. If we compare Fig. 2(b) with Fig. 2(a), we see that for $\langle R\rangle$ between 2.0 and 2.3, one can also find a nearly linear correlation between $\Delta\omega_{\mathrm{LO}}$ and $\langle R\rangle$. What will happen when $\langle R\rangle<2.0$? This question should eventually be settled experimentally. I would expect that $d\Delta\omega_{\mathrm{LO}}/d\langle R\rangle$ would decrease, as the $R=1$ anion perovskites are not antiferroelectric.[30] In the language of the present network model, for $\langle R\rangle<2.0$, self-organization should be even more important than for $\langle R\rangle>2.0$.

Before we leave Fig. 2, we should note an important feature of Fig. 2(a). It is well known that there are large qualitative differences between the properties of underdoped and overdoped samples of a given cuprate (several examples are discussed in the next section), so that optimal doping ($z=1$, $T_c=T_c^{\max}$) has critical properties. The plot of Fig. 2(a) similarly shows a cusp in $T_c^{\max}(\langle R\rangle)$ at $\langle R=2\rangle$, which suggests that $\langle R\rangle=2$ is a supercritical point where $T_c^{\max}=(T_c^{\max})^{\max}$. In fact, the Fermi lines of cuprates with $\langle R\rangle>2$ all appear to be quantitatively consistent with conventional self-consistent band theory, but this theory fails qualitatively for $\langle R\rangle<2$ (Sec. VI). For $\langle R\rangle>2$, the interplane filamentary topology shown in Fig. 1 is consistent with band theory, but an additional, more complex intraplane filamentary topology could be required for $\langle R\rangle<2$.

One more factor should be considered, and that is the dopant sites themselves. In the presence of multiple nanophases, there may be multiple dopant sites for the same dopant, one for each nanophase. The natural candidate for the negative U (superconductive) interstitial O_x in BSCCO in a superconductive region is a split apical (Cu-O-Bi) site B, which apparently generates polaronic structure in the midinfrared, with a line shape virtually identical to that predicted by theory;[31] B could be associated with a narrow half-filled impurity band pinned to E_F, with charge $Z_B=-1$.[32] The pseudogap regions dominate I-V STM characteristics near $E_F-0.9$ V, and there a negative U dopant site A is found near Sr,[33] and here $Z_A=-2$, that can be assigned to pseudogap regions. Evidence that there is indeed a B site that generates an electrically active impurity band is apparent in the dramatic increase in $N(E_F)$ (Ref. 34) as T increases across T_c. Neutron scattering[35] has provided indirect evidence that there are two independent dopant sites, as those sites are surely responsible for the giant softening of the zone-boundary z-axis polarized phonon observed in metallic LSCO relative to insulating LCO. The phonon peak is anomalously wide, as one would expect if there are two inequivalent Sr doping sites, just as there are two different gap regions. There is also old evidence that only half of the O_δ dopants in $\mathrm{Hg_2CuO_{4+\delta}}$ are electrically active.[35] Another intriguing possibility is that in $\mathrm{Bi_2Sr_2CuO_{6+x}}$ (BSCO), which resembles BSCCO except that it has only one Cu layer and no central Sr layer, there is only one important site for the interstitial O, and this is the electrically active site B in the apical oxygen layer.

The reactions of HTSC experts to Fig. 2(a) have varied from surprise (materials scientists: never seen anything like this) to incredulity (theorists: how can such a simple configuration coordinate be so successful when it is completely independent of the atomic potentials and the lattice structure?). It is important for the reader to realize that Fig. 2(a), which shows the least upper bound function $T_c^{\max}(\langle R\rangle)$, is both comprehensive and accurate. The success of this plot is unprecedented,[2,7] which is why it has remained "hidden in plain view" for so long, and this success *transcends* all the details that are discussed in the following sections, including complex erratic pseudogap and/or superconductive gap (gapology) issues. At the same time, this success tells us that a designed dopant-centered network model is the logical point of departure for discussing these details. While a full microscopic theory is still to be developed, the details are already so spectacular that they fully deserve to be discussed using a dopant-centered filamentary network model. Even at the qualitative level of this paper, the connected Lagrangian off-lattice network model illuminates many interesting features of the rich cuprate database that are inaccessible to Newtonian lattice models and provides a comprehensive framework for analyzing the very large cuprate database.

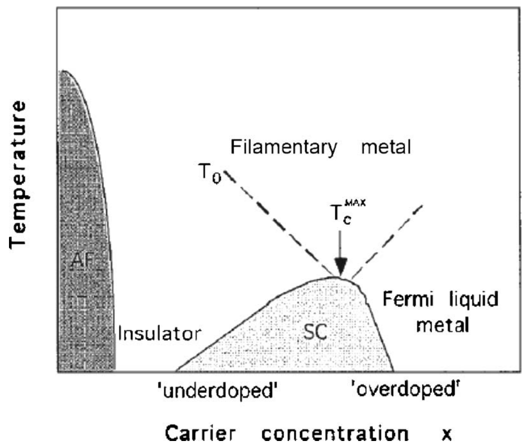

FIG. 3. A sketch of the "standard" phase diagram for HTSC, including lines for the pseudogap defined in terms of magnetic susceptibility and electrical resistivity, modified from Ref. 38.

V. BROAD IMPLICATIONS OF PHASE DIAGRAMS

It is customary, in many theoretical papers, to begin an elaborate mathematical discussion by showing a token phase diagram borrowed from an experimental paper, such as the diagram shown in Fig. 3.[36] The diagram shows several phases: an antiferromagnetic (AF) phase near dopant concentration $x=0$, an intermediate phase that is superconductive and exhibits non-Fermi-liquid normal-state transport properties, an unspecified pseudogap phase, and a Fermi-liquid nonsuperconductive phase at large x. There is, however, much more in this phase diagram than merely a rich variety of phases.

First, there is the question of the relevance of the AF phase to the superconductive phase, as the two are separated by the pseudogap phase (supposed here to be partially antiferroelectric). There is no doubt that NiO is a strongly AF material over a wide range of alloying with other oxides, but in the cuprates, the AF phase disappears at small values of x (<0.03 in LSCO, see below). Why does this happen? As we have seen from the master curve in Fig. 2(a), the cuprates are marginally stable elastically. The AF instabilities associated with half filling of the Cu $d(x^2-y^2)$-O $p(x,y)$ conduction band compete with, and are easily replaced by, charge-density waves based on 2×1, 2×2, etc., antiferroelectric reconstructions,[6] and this will occur at very small values of x because of the very large numbers of degrees of freedom in the 3 nm glassy nanodomains observed by STM.[5] In other words, the pseudogaps in the regions that form the maze through which dopant-based filaments percolate are almost surely CDW (or Jahn-Teller) pseudogaps, and not AF pseudogaps.

This is a very important observation, because theories are appearing that seem to resemble the present theory yet are fundamentally different from it. For example, a recent theory[37] without attribution borrows for its subtitle the title of my 1989 book,[18] and it discusses topological aspects of its model "based on Anderson's idea of the resonating valence bond, and argues that it gives a qualitative account of the data," but the topology is completely different. The model assumes that the host lattice is AF and that the dopants are not interstitial but are placed on lattice sites; these sites are then averaged over. This translationally invariant all-lattice spin model has several gauge symmetries and is called a "doped Mott insulator." It treats phonons as merely a thermal nuisance and is technically similar to spin-glass models of network glasses, which beg the question of self-consistent, space-filling network connectivity and tell us little or nothing about the physics of real off-lattice glasses such as window glass.[1,22]

Electric dipoles have generated filamentary paths in successful off-lattice simulations of the Boolchand intermediate phase (also not cited in Ref. 37). The simulations exhibit quite generally the combined effects of space filling and competing long- and short-range forces in the formation of the Boolchand intermediate phase.[38] In the AF model, these space-filling off-lattice electric quadrupoles have been replaced by spins on a lattice; of course, lattice models can contain a metal-insulator transition, but as they permit only one connectivity phase transition, they cannot explain the formation of the intermediate phase. Moreover, magnetic spins have pseudovector symmetry, while electric quadrupoles are symmetric tenors. We shall see in later sections that the mysterious magnetic precursive effects observed in HTSC are, in fact, closely correlated to lattice strains indicative of strong off-lattice interactions of electric quadrupoles. The latter first order into loops and then pass through a mean-field topological ordering transition near the onset of superconductivity. On behalf of the doped Mott insulator theory,[6,37] it should be said that, unlike string theory (where the physics is "not even wrong"), its physics is "completely wrong," as shown by multiphonon fine structure seen in recent very-high-resolution ARPES experiments.[38] Alternatively, the mathematics of both string theory and Ref. 37 are "interesting," but not "amusing." Many other popular "toy" models of HTSC, such as *t-J* and Hubbard models, are also mathematically interesting, but not amusing, as they do not attempt to analyze the strong disorder and dopant networks that are characteristic of all HTSC.

There is much more to be learned from the standard cuprate phase diagram by comparing it to the phase diagrams of other materials that undergo superconductor-insulator transitions, notably thin strongly disordered W-Si films and the $(\mathrm{Ba,K})(\mathrm{Pb,Bi})\mathrm{O}_3$ family.[39] In both cases, T_c increases to its largest value as the transition is approached with decreasing doping. The dopants are nearly randomly disordered, and the effective-medium (or virtual-crystal) approximation is valid. The increase in T_c occurs because near the transition, dielectric screening of the attractive electron-phonon interaction breaks down, and at the transition, some changes occur in the internal structure that open an insulating gap. There are indications of some internal ordering of the K dopants (incipient breakdown of the effective-mass approximation) in the $(\mathrm{Ba,K})\mathrm{BiO}_3$ case[39] with increasing T_c.

Ando *et al.* obtained very sophisticated features of the cuprate phase diagram by studying the T dependence of the planar resistivity in the normal state[40] (Fig. 4). Plots of the *ab* planar resistivity $\rho_{\mathrm{ab}}(x,T)$ of $\mathrm{La}_{2-x}\mathrm{Sr}_x\mathrm{CuO}_4$ exhibit *two* Ando lines (I and II) $d^2\rho(x)/dT^2=0$. Line I is diagonal and defines the pseudogap temperature $T_p(x)$, while line II de-

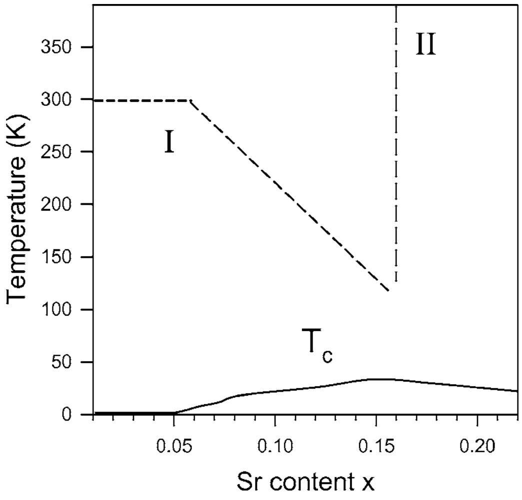

FIG. 4. The planar resistivity $\rho(x,T)$ phase diagram of $La_{2-x}Sr_xCuO_4$ (LSCO), after Fig. 2(c) of Ref. 40. Two lines zeros of $d^2\rho(x)/dT^2$ are marked I and II, as discussed in the text.

fines a critical crossover very nearly fixed vertically at optimal doping, $x=0.15$. Line I has a corner near $x=0.06$, where the metal-insulator transition occurs; it is possible that this corner is also connected with a crossover from an AF pseudogap to a CDW pseudogap (see above). The *rectilinear* (not curvilinear) nature of both Ando lines is a strong evidence for the percolative character of the (super)conductive paths formed by the internal filamentary network, as such rectilinearity is characteristic of percolative phenomena in strongly disordered (glassy) systems.[41] The nature of the critical crossover (line II) at optimal doping is revealed by the experiments (using samples prepared in Ando's laboratory) that are the subject of the next section.

There are other interesting aspects of the cuprate phase diagram, notably the Rohler bulge (~0.1%) in the CuO_2 planar lattice constants in the intermediate phase.[42] One might have thought that the superconductive condensation due to attractive electron-phonon interactions would have caused a lattice contraction in the *xy* plane, so this bulge could be surprising. However, we saw above that the strong attractive *s*-wave interactions occur at the interlayer negative *U* dopants, and these cause local contraction of the interlayer spacing. Since the unit-cell volume remains nearly constant (normally Poisson's ratio is negative), the interlayer contraction causes a bulge in the planar lattice constants.[12] An interesting feature of the bulge is that at optimal doping, $x=0.15$, it reaches a sharp minimum at $T_0=190$ K.[43] The significance of T_0 will be discussed in Sec. VII. Further, there is also a positive bulge (~0.1%) in the temperature dependence below 150 K of the mean-square *relative* displacements determined by the correlated Debye-Waller factors σ^2 of the Cu-O bonds by extended x-ray-absorption fine structure (EXAFS) at $x=0.1$, which is measurably weaker (<0.03%) at $x=0.2$.[44] The meaning of this difference between under- and overdoped networks is discussed later in Sec. VI.

VI. EMERGING FERMI ARCS AND CROSSOVERS AT OPTIMAL DOPING

HTSC characteristically exhibit three phases; an insulating phase (dopant concentration x in the range $0<x<x_1$), an intermediate superconductive phase with anomalous normal-state transport up to temperatures of ~700 K ($x_1<x<x_2$), and a nonsuperconductive metallic or Fermi-liquid phase ($x>x_2$).[1] The superconductive transition temperature $T_c(x)$ reaches a maximum near the center of the intermediate phase at the optimal doping $x=x_0$.

ARPES experiments[45] on LSCO ($x_1=0.06$, $x_2=0.22$, and $x_0=0.16$) showed metallic behavior in the Fermi arc even at $x=0.03$ (insulating phase) beginning in the nodal (π,π) gap direction and spreading smoothly over a wider angle as x increased. The spreading behavior is explained by self-consistent field band calculations.[45] However, similarly good agreement of Fermi-surface areas with doping levels was not obtained[45,46] for $Ca_{2-x}Na_xCuO_2Cl_2$ (NCCOC). Note that $\langle R\rangle$(NCCOC)<2, so that NCCOC lies on the opposite side of the percolative connectivity peak in Fig. 2(a).

If we look closely at Fig. 6(a) of Ref. 45, which plots the apparent doping concentration x_{FS} inferred from Fermi-surface geometry against the actual doping level x, we see something not discussed there. At optimal doping, $x=0.15$, the mean-field band model agrees well with experiment, as it should. However, $dx_{FS}/dx=1.4(1)$, and not 1.0; the filling of the Fermi area is "inflated." The band model has been corrected for changes in geometry with doping, so it is not a rigid-band model, and these geometrical corrections do not explain the inflation. However, the fraction of electrically active *B* dopants (Secs. IV and IX) could increase with x, as these Fermi-energy dopants are softer than the ones at lower energies, which would explain the inflation.

Band theory does not explain the doping dependence of the apparent nodal k_F in NCCOC. Historically this failure was explained in terms of antiferromagnetic pseudogaps and various parametrized toy models (*t*-*J* and Hubbard), all based on mean-field theory.[46] However, as the observed ARPES spectra of NCCOC are qualitatively different from those of LSCO (where the mean-field self-consistent band model works well), the first question to be raised is whether the mean-field assumption itself is justifiable. We already know from Fig. 2(b) that HTSC is correlated not with antiferromagnetic pseudogaps but with antiferroelectrically softened LO phonon modes (Jahn-Teller distortions). Moreover, recent STM data on NCCOC (discussed in the Appendix) show a bilinear grid structure with both similarities and differences from BSCCO.

It appears that the simplest model for these differences is that the band theory description of the CuO_2 planes survives the formation of nanodomain structures and bilinear grids in BSCCO ($\langle R\rangle>2$), but not in $Ca_{2-x}Na_xCuO_2Cl_2$ ($\langle R\rangle<2$). In other words, the electronic structure of the metallic filaments changes qualitatively at $\langle R\rangle=2$, which acts as a configurational critical point (see the Appendix). The splitting of the ARPES bands (Fig. 2 of Ref. 46) into a strong and Franck-Condon broadened *A* band near $E_F-0.5$ eV with a weak shoulder *B* close to E_F may be explained in terms of Na doping which produces a Na-based impurity band B near the top of the valence band. As x increases, this leads to the apparent shifts in ARPES band A, which are described[46] in terms of a shift in chemical potential. There are also important qualitative differences for $\langle R\rangle > (<) 2$ in spatially separated bilinear filamentary nanostructures (the Appendix), and these can easily explain the otherwise quite puzzling "small" Fermi nodal k_F of NCCOC.[46]

VII. COMPARISON WITH OTHER THEORIES

There is a very wide range of lattice-based mean-field theories of HTSC,[47] in fact, a too wide range. The most striking features of these lattice-based mean-field models are their reliance on adjustable parameters and their inability to produce substantive results, such as those discussed here in the master curve for $T_c^{\max}(\langle R\rangle)$ [Fig. 2(a)] and the correlation of $T_c^{\max}$ with $\Delta\omega_{\mathrm{LO}}$, or to explain the isotope effect. Analytically the reason for this is clear: the lattice-based models incorporate nearest-neighbor coordination numbers, but these numbers represent only the laboratory-time mean-field average of dynamical configurations. Most of the time, the atoms are displaced from their marginally stable lattice sites in such a way as to form a percolative off-lattice dopant network involving interstitial dopants that optimizes dielectric screening of internal electric fields fluctuating on picosecond time scales. In my view, these difficulties are unavoidable, because these lattice models attempt to describe the exponential complexity of HTSC in the cuprates using analytical models. Unlike analytical models, topological models are not adorned by elaborate algebra, but they also consistently describe the connectivity of the internal off-lattice dielectric network, and they contain no adjustable parameters. Their great strength lies in their ability to identify and even predict the essential qualitative features of complex off-lattice problems; here, these problems arise from the need to identify the essential features of many-body dopant configurations relevant to a given experiment.

The Fermi arcs identified by ARPES have attracted great theoretical interest, previously discussed using analytical (polynomial) models; it is therefore useful to compare these analytical models with the present topological model, particularly with respect to qualitative features. Although by now it is abundantly obvious that electron-phonon interactions cause high-temperature superconductivity and that gas- or liquidlike quasiparticle models cannot account even qualitatively for the dependence of the phonon kink on x and isotopic mass,[27,28] almost all the mean-field models that claim to explain the Fermi arc in underdoped cuprates invoke fictive spin (not phonon) degrees of freedom.[48,49] Strong claims are made for these models:[49,50] they contain the "essential" physics of the cuprates, the momentum dependence of their quasiparticle states is "essentially" that observed by ARPES, etc. Similarly, strong claims have been made for Fermi-liquid models with strong spin-relaxation channels.[51]

A striking feature of all the spin-dependent mean-field (Fermi-liquid) models is that they purport to explain optical data (which reflect almost entirely electric dipole transitions, with oscillator strengths determined by orbital coherence) in terms of both spin and orbital degrees of freedom, yet they never mention the awkward fact that the atomic spin-orbit coupling $\lambda(\mathbf{L}\cdot\mathbf{S})$ parameters λ for O $2p$ and Cu $3d$ states are ~ 0.01 eV, which is negligibly small compared to the orbital bandwidths $W \sim 1$ eV. In these "strong-coupling" Hubbard mean-field models, the spin and orbital degrees of freedom are coupled as artifacts of projection procedures driven by the Coulomb repulsion parameter U, assumed to be $\sim 10W$. These "central cell" (short-range) projection procedures involve many uncontrolled approximations that are probably incompatible with coherent intercellular (long-range) orbital motion, and the gradual appearance of the Fermi arc may be merely an artifact of the projection procedures used. (Note that in the parallel classical problem of mechanical elasticity, phase changes from floppy to rigid, and in the mean-field approximation *there is no intermediate phase*.[52] It seems likely that were the quantum models to be treated exactly in mean field, the intermediate phase would disappear there as well; it appears as an artifact derived from smoothing out a first-order mean-field phase transition.) Of course, no justification has ever been given for abandoning the ideas of self-consistent one-electron calculations for these uncontrolled approximations, which, to my knowledge, have never been confirmed experimentally for any carefully studied simple material. These self-consistent one-electron calculations are the basis for all successful predictions of optical and photoemission spectra of solids,[53,54] and they have successfully predicted matrix element effects in cuprate photoemission spectra.[55] If the reader scans the present paper for the phrase "space filling," the reader will find many applications of the space-filling concept that are simply not accessible by analytic methods. For example, recently, effects of space filling have also been identified in the asymptotic oscillations of partial radial distribution functions of glasses and glass-forming liquids, which are specific to these materials but are, in general, absent from most nonglassy complex materials.[52]

VIII. PICOSECOND REFLECTANCE RELAXATION

The emphasis in the present self-organized (adaptive, not random) percolation model on formation of dopant filaments apparently requires a "Maxwell demon" to identify such dopants, especially as optical experiments involve wavelengths much longer than the nanodomain dimensions identifiable only by large area, high-resolution scanning tunnel microscopy (STM) studies.[5] However, time-resolved relaxation studies have proven to be a powerful tool in studying network self-organization in both molecular and electronic glasses,[1,56] and elegant pump-probe reflectance relaxation studies[57] at 1.5 eV have revealed picosecond anomalies in LSCO, ($x_1 = 0.06$, $x_2 = 0.22$, and $x_0 = 0.16$) that closely parallel the ARPES anomalies, with an abrupt change in relaxation time at optimal doping.

It seems surprising that a simple reflectance measurement, which averages over all $\mathbf{k}$ values involved in interband optical transitions, can yield an anomaly very similar to that obtained by the much more refined and precise ARPES $\mathbf{k}$-resolved technique; this is possible because there are some very subtle aspects to pump-probe time-resolved relaxation

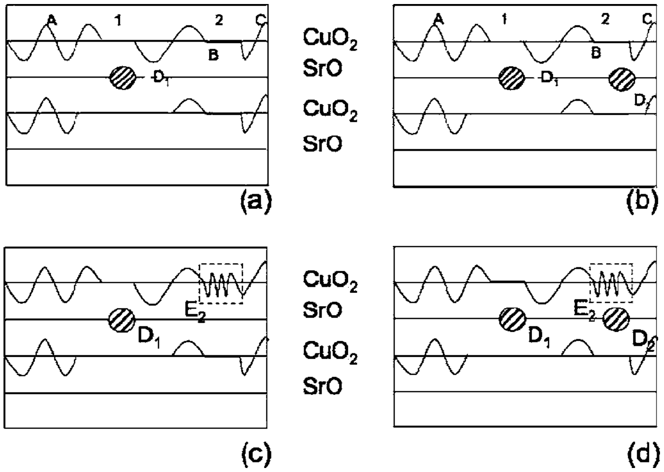

FIG. 5. The percolative model of Fig. 1 is redrawn here to illustrate the effects on path coherence due to crossover from underdoped to overdoped. The metallic regions of the CuO_2 planes are indicated by wavy curves; these regions are separated by semiconductive nanodomain walls, indicated by straight lines. In (a), we have two such walls, marked 1 and 2. In wall 1, there is a dopant in the SrO layered labeled D_1. A coherent filamentary current path can go from A to B in the CuO_2 plane by utilizing D_1 as a bridge to bypass wall 1. The filament ends at B. In (b), a second dopant D_2 has been added to wall 2, so that now the filament continues from A through B to C. In (c), D_2 has been replaced by a surrogate excitonic bridge E_2; this structure explains the positive value of $\Delta R/R$ observed in underdoped samples in picosecond relaxation experiments (Ref. 54). Finally in (d), we have the overdoped case, where the exciton overlaps a dopant, locally destroying the coherence of the filament and giving rise to a negative value of $\Delta R/R$.

studies in self-organized glassy systems.[56] These are illustrated in Figs. 5(a) and 5(b). The electron-hole pair created by photon absorption relaxes rapidly (femtosecond time scale) to a metastable excitonic state which then relaxes much more slowly, probably nonradiatively (phonon emission), on a picosecond time scale. The experimental relaxation data,[57] reproduced for the reader's convenience in Figs. 6(a) and 6(b), refer to this second regime. There are not one but two surprises in these data. First, $\Delta R(x)/R$ smoothly reverses sign at $x=0.16=x_0$, and second, the relaxation time τ abruptly drops from 20 ps in the underdoped regime $x<0.16=x_0$ to ~ 2 ps for $x \geqslant 0.16$. As emphasized in Ref. 57, this is strongly reminiscent of the abrupt crossover in $Z(x,\pi/4,E_F)-Z(x,0,E_F)$ in Fig. 2(c) of Ref. 45. At the same time, it is hard to understand how this abrupt drop can be associated with a "saddle-point" peak in the quasiparticle density of states $N(E)$ pinned to E_F at $x=x_0$. (In a quasiparticle band model, τ would reach a minimum at $x=x_0$ and then recover for both $x<x_0$ and $x>x_0$.) The self-organized (not random) filamentary percolation model, with its strong local-field corrections, readily explains both of these results (surprising and *basically inexplicable* in a mean-field quasiparticle context).

Because the pump and probe both have energy of 1.5 eV, this experiment detects changes that occur because of addition of a metastable exciton to the filamentary network. The exciton is metastable because it has been added to a semiconductive nanodomain wall (excitons added to the metallic nanodomains decay on the femtosecond time scale), and it decays by "leaking out" (tunneling) to the metallic regions. The positions occupied by the metastable exciton are not all equivalent, even though the probed single-particle exciton energy remains fixed at the pump energy of 1.5 eV. The exciton is highly polarizable, and the free energy of the filamentary network depends on the position of the exciton. For $x<x_0$, the exciton diffuses to positions that minimize the system's free energy by increasing the conductivity of the filamentary network. Thus, the exciton functions as a surrogate dopant, increasing the length and connectivity of coherent filaments and, hence, increasing the reflectivity, $\Delta R/R>0$. However, for $x>x_0$, the filaments have already filled the available phase space (optimized glass networks are space filling and "incompressible"), and when excitons are added, they function again as dopants, but this time as excess dopants, disrupting filamentary network segments and producing incoherent Fermi-liquid-like regions.

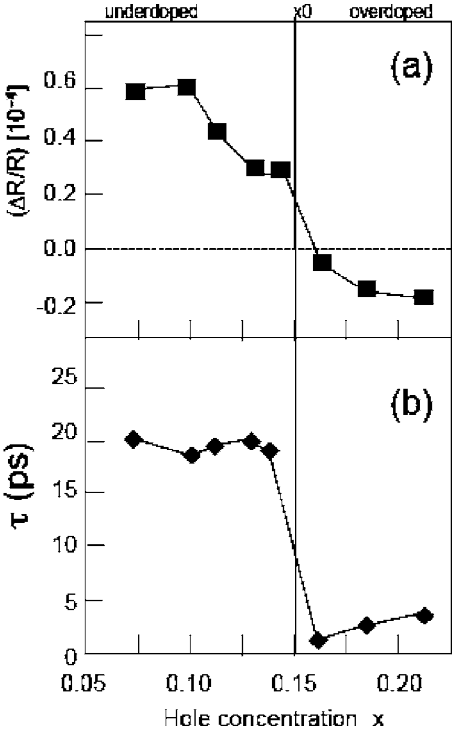

FIG. 6. For the reader's convenience, the relaxation data from Ref. 57 are redrawn here: (a) $\Delta R(x)/R$ changes smoothly with x and reverses sign at $x=x_0$; (b) $\tau(x)$ changes abruptly (essentially a step function) at $x=x_0$. The picosecond time scale of $\tau(x)$ implies that phonons play an essential part in the relaxation. Because the relaxation is essentially dielectric relaxation, spins are irrelevant.

The evolution of the filamentary network with doping is easy to understand: the highly mobile dopants self-organize to form conductive (electronically coherent) segments. By forming such conductive segments, the dopants lower the sample free energy by better screening internal electric fields in this strongly ionic material. The anisotropy of the energy gaps tells us that the antinodal (nodal) directions $\alpha=0$ $(\pi/4)$ are the directions of strongest (weakest) electron-phonon interactions. Thus, the nodally oriented segments have the lowest scattering and the highest conductivity, and the segments that are formed at small $x=0.03$ are therefore oriented predominantly in the $\alpha=\pi/4$ direction. With increasing x, the segments begin to percolate at $x=x_1$ to form a metallic network. Because of the presence of a high density of Jahn-Teller distorted insulating islands (large pseudogaps[5]), the percolative paths become sinuous, and to avoid filamentary overlap, the occupied Fermi-surface arc spreads to larger values of $|\alpha-\pi/4|$ with increasing x. Note that these filamentary states are loosely bound or pinned to the dopants outside the metallic planes. The host momentum spectrum remains that of the metallic patches in the metallic planes, which is why addition of dopants shifts the Fermi arc radially in accordance with doping carrier concentrations and self-consistent field band calculations.[46] Note that the filamentary paths are three dimensional, and are not confined to the metallic planes; when projected onto these planes, the filamentary states lie in the energy gaps of the nanodomain walls. Without these walls, the filamentary states could not be formed.

There are two reasons why $\Delta R(x)/R$ changes smoothly with x. First, the high-conductivity sites, with $\alpha=\pi/4$ filamentary tangents, are occupied first, and the lower conductivity sites (increasing $|\alpha-\pi/4|$) are then filled with increasing x. Second, note that for $x<x_0$, the exciton must diffuse from its initial region to find the best filamentary site, and that this is an easier task for strong underdoping, when the filaments are nearly oriented in $\alpha=\pi/4$ channels, than near optimal doping, when the filaments have become sinuous, and the entire network must reconfigure itself to improve its coherent conductivity. For $x>x_0$, the disruption is minimized for surrogate insertion near $\alpha=0$ oriented filamentary tangents, where the local conductivity is less than in $\alpha=\pi/4$ channels. That is why the magnitude of $\Delta R/R$ is smaller for strong overdoping than for strong underdoping. One can add that a semiclassical simulation of coherent filamentary percolation could be carried out in the context of directed percolation, with angular weighting factors. Such a simulation would be considerably more complex than the mechanical simulations of Ref. 52, and it lies outside the framework of this paper.

The situation for $\tau(x)$ is different. For $x<x_0$, decay of the exciton must occur through a Franck-Condon configurational barrier (the exciton abandons its surrogate coherent filamentary function and decays into an incoherent state), which leads to a large τ. For $x>x_0$, the exciton tunnels from an incoherent state in the semiconductive wall to another incoherent state in the adjacent metallic nanodomain. Because both states are incoherent, the Franck-Condon configurational barrier almost disappears, and the decay takes place on a picosecond (one phonon) time scale (ten times faster than for $x<x_0$).

The measured abrupt drop in the average value of τ by a factor of 10 at $x=x_0$ can be estimated as follows. According to the discussion at the end of Sec. II, in the metallic region $x>x_0$, the energy-level spacing in a nanodomain is of order W/N, where $W\sim 1$ eV is the valence bandwidth and N is the number of unit cells in the nanodomain. In the filamentary region $x<x_0$, the intrafilamentary energy-level spacing in a nanodomain is of order $W/N^{1/3}$, so it is much larger. All other things being equal, Fermi's golden rule for transition rates says that the ratio of the relaxation times will scale as $N^{2/3}$. This gives $N\sim 30$, which is consistent with the observed nanodomain dimension of 3 nm at optimal doping.[5]

A related effect, superconductivity-induced optical reflectivity spectral weight shift $\Delta\mathrm{SW}_{\mathrm{sc}}(x)$ below 1.25 eV in BSCCO, is also a skewed parabola that tracks the parabolic $T_c(x)$.[58] This behavior is exactly what is predicted by the three-phase filamentary model: from underdoped to optimally doped, $\Delta\mathrm{SW}_{\mathrm{sc}}(x)$ increases as the number of filaments increases to its space-filling limit. In the overdoped samples, $\Delta\mathrm{SW}_{\mathrm{sc}}(x)$ decreases rapidly, mirroring 1.5 eV pulse-probe reflectivity and relaxation time drops,[57] because of interfilamentary scattering in Fermi-liquid patches.

IX. NANODOMAINS AND DOPANT SITES

Wide-area STM experiments on $\mathrm{Bi_2Sr_2CaCu_2O_{8+x}}$ (BSCCO) (Ref. 5) have opened a unique window on the nanodomain gap structure, which has surprised almost all the theorists committed to models of HTSC based on homogeneous lattices. Fortunately, for theorists, the geometrical limitations of STM studies of micaceous surfaces still leave many questions unanswered. The internal gap structure near the surface is projected on a single plane, so that even if one assumes that only the uppermost unit cell dominates the observations, the gap patterns of BSCCO are still superpositions of patterns from at least two $\mathrm{CuO_2}$ planes and, probably, two BiO planes as well. The gaps are associated with off-lattice O_x interstitials, which are not easily observed, and the role of these interstitials is not easily established.

Before one can suggest a theoretical model for dopant siting, one should first consider the main features of the observed patchy nanodomain structure. The patches are typically $d\sim 3$ nm in diameter, and this length is independent of dopant concentration from under to overdoped.[5] It seems likely that the sizes of the patches are set by the self-limiting effects of internal stress, as these often limit cluster sizes in glasses (boson peak[59]). Because there are two kinds of gaps, it seems reasonable to assume that there are two kinds of interstitial sites—one associated with pseudogap nanodomains and one associated with superconductive gap nanodomains.

McElroy *et al.*[59] have recently reported a remarkable observation: they have succeeded in identifying one of the two possible oxygen interstitial dopant sites, labeled A and B. They were able to localize the A dopants using enhanced currents in their I-V characteristics at -0.9 V below the Fermi energy E_F. The A dopant sites (located laterally with a resolution better than 1 A) are positively correlated with large values of the strongly inhomogeneous gap parameter $\Delta(\mathbf{r})$ and are presumably associated with the pseudogaps, generally larger than superconductive gaps. These states are coupled to the CuO plane through apical oxygen sites.[59] The B dopant states of the latter should pin E_F, as they do in semiconductor impurity bands, and not be 1 eV below it, where they are part of the electrically inactive part host framework. [60] Almost all of the STM data have been taken at low T, but recent data taken near T_c have shown a very

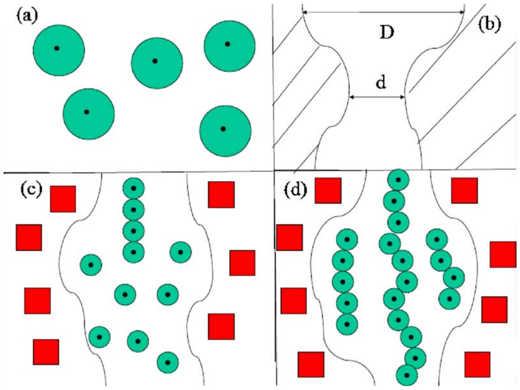

FIG. 7. (Color online) (a) Randomly distributed dopants (black dots) in a homogeneous background. Ionic fluctuations are screened dielectrically in regions here idealized as circles. (b) Channel geometry formed by pseudogap regions, with variable widths typically ranging from d to D. [(c) and (d)] The black dots are O_x^-, while the rectangles are the electrically inactive O_x^{2-}, and the circles are the electrically active O_x^-. (c) Even at low doping densities, it is energetically advantageous for the electrically active dopants (circles) to form linear segments (upper chain). (d) More than one linear segment can form in wide regions of a channel; when the segments lengthen, narrow regions act as bottlenecks limiting the number of percolating segments.

interesting effect: increasing T by 14% across T_c produced no measurable change in the residual pseudogap distribution in an optimally doped BSCCO sample, but greatly enhanced $N(E_F)$.[61] This is a possible signature of B dopants. A recent note is the idea that there should be two such sets A and B of dopant sites has also been developed elsewhere.[61]

X. PRECURSIVE MAGNETIC EFFECTS

One of the striking anomalies in HTSC is that with decreasing T, there are two very large precursive magnetic effects: the giant Nernst effect in the thermomagnetic power[62] and field-enhanced diamagnetism, with composition dependence parallel to that of the Nernst effect[63] but shifted toward underdoping relative to HTSC itself. To understand these effects, let us look at hierarchical trends in possible sets of dopant configurations, assuming that the dopants minimize the free energy by optimally screening internal ionic fields.

The first point is that between the pseudogap nanodomains decorated by A dopants, there will be channels occupied by B dopants. In other words, the pseudogap regions represent barriers in a maze around which filamentary paths centered on electrically active dopants must percolate. Thus, the B dopants are not randomly distributed [Fig. 7(a)]. Instead, as with all disordered percolative structures, local structure is characterized by its longitudinal and transverse features [Fig. 7(b)]. In the conducting regime, there are local curvilinear channels that are longitudinally open, but transversely confined, with a variable spacing between the pseudogap confinement walls. Within the tetragonal framework of conductive CuO_2 planes, one can distinguish two principal directions, the (10) ones parallel to CuO rows and the (11), angularly between the (10) and (01) CuO rows. Electron-phonon scattering is strongest parallel to CuO rows, so one expects that mean free paths will be longer in the (11) directions than in the (10) directions. In other words, the Fourier grid of the host lattice lifts the planar angular degeneracy of the glassy dopant network.

There are several factors that optimize dielectric screening. The screening is approximately exponential (classically, Debye-Waller, quantum mechanically, and Thomas-Fermi) around each dopant, but in our figures, for simplicity, this screening charge is represented by a constant charge density with a radial cutoff (a disk in plan view). The actual "fuzzy" screening charge spreads out and overlaps the screening charge of nearest neighbors. The overlap is favorable for screening because there is metallic charge delocalization and higher conductivity along filamentary paths. However, if the charges overlap too much, then the volumes (or areas in plan view) are duplicated, and some screening energy is lost to redundancy. This factor tends to favor more nearly linear metallic filaments, which are already favored by the (10) linearity of the pseudogap barriers.

Another factor is the variability of channel widths. Suppose we call the wide channel regions ponds, and the narrow ones bottlenecks. B dopants will gain more energy from screening ponds than from screening bottlenecks, as confinement in the bottlenecks means that some of their screening charge will spread out into pseudogap regions, where the lattice is stiffened by the pseudogap, and hence the marginal instability of ionic fluctuation amplitudes is reduced. Because of the exponential fuzziness of the screening charge, they will also gain more energy from screening larger ponds than from screening smaller ones, especially as the former are well suited to the formation of dopant loops that can carry large screening ring currents, as the latter are not scattered by filamentary ends.

Another characteristic feature of ponds and bottlenecks is that they will generate loops of dopant centers in the ponds, as well as strings or filaments of dopant centers that extend from pond to pond through a bottleneck. Which feature is favored depends on details of channel geometries, the relative magnitudes of end energies, and the linearity energy. See Fig. 8 for examples of some of the possibilities.

Each of these topological features has its own length scale, and with each length scale, some kind of mean-field transition occurs. These cascading mean-field transitions eventually lead to superconductivity, but they also correspond to hierarchies of stress-induced and strain limited transitions of the martensitic type. The existence of such multiple length scales is a quite general consequence of off-lattice relaxation, and Ahn *et al.*[64] and Jacobs and Thorpe[65] have discussed it frequently. Because the cuprates are spectacularly soft, with $R \approx 2.0$ (Fig. 2), the effects here are larger and better defined than in other soft lattices, for instance, in the traditional ferroelectric and ferroelastic perovskites (such as $BaTiO_3$) where $R \approx 2.4$.

Let us start with the highest temperatures, where filamentary loops begin to form. The virtual diamagnetic currents associated with isolated loops can be detected by spin-polarized neutron scattering, and such scattering has been observed.[66] The formation temperature T_{mag} in $YBCO_{6+x}$

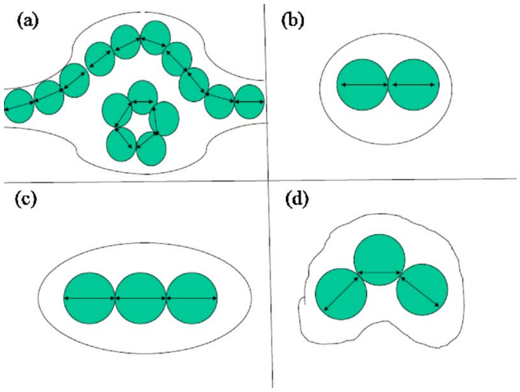

FIG. 8. (Color online) (a) When there is free area in wide regions which are shorter than shown in Fig. 1(d), closed loops (hydrodynamic eddies) are energetically favored at high temperatures. (b) Adjacent nonoverlapping dopant pairs screen larger areas. Linear segments (c) screen larger areas than curved segments (d). In these figures, double arrows in each circle represent enhancement of screening along enhanced polarizability axes due to charge overlap (not shown).

ranges from 300 K at $x=6.5$ to 170 K at $x=6.75$, so that T_{mag} is similar to a pseudogap transition temperature obtained from linearity of the planar resistivity. The mechanism proposed here, involving dopant loops, is different from the one suggested in Ref. 66, where only the host lattice is discussed, and translational invariance is supposed to be required. However, the dopant spacings in loops will also be regular, as these must be in registry with the lattice; this weaker condition of registry is enough to cause the spin-polarized neutron scattering to peak at Bragg peaks. The signals produced by dopant registry are much weaker than those produced by translational invariance, which explains why the observed signals are also very weak.[66] Moreover, the present model explains why T_{mag} is similar to a pseudogap transition temperature, as the loops will begin to form as soon as the channels and ponds form. There is no obvious connection between T_{mag} and a resistivity pseudogap transition temperature in the translationally invariant model.[66]

It is noteworthy that the temperature dependence of the spin-polarized neutron scattering does not have the mean-field form $f(1-(T_{\mathrm{mag}}/T)^2)$ expected from translational invariance, i.e., microscopic homogeneity. Instead, the temperature dependence[66] is ragged and more nearly linear in T_{mag}/T. This is consistent with the kind of broadening one would expect from a glassy model with a broad distribution of pond sizes. As T is lowered, adjacent ponds will be filled more often, and strings will appear connecting such ponds. In the hydrodynamic analogy, eddies will appear in adjacent ponds, and streaming will carry particles from one eddy to the next. The streams and eddies are always coupled, and in the hydrodynamic case, there are procedures for determining the coupling for known channel geometries.[67]

Similarly, in the presence of crossed electric (or thermal gradient) and magnetic fields, the vorticity of carriers in these loops can be activated to jump across the bottlenecks to loops in adjacent "ponds." Because the hopping distance is large and the pinning of the vortices by the soft host lattice is weak, this mechanism will inevitably lead to a giant Nernst effect in the thermomagnetic power. This effect has been observed[62,63] in both BSCCO and LSCO, and it peaks near $x=0.11$, in other words, well above the MIT at $x=x_c=0.06$, yet well below optimal doping $x=x_0=0.16$, near $x=(x_c+x_0)/2$, which would be the expected value for a plausible channel aspect ratio of 2. The onset temperatures at optimal doping x_0 are 150 K (BSCCO) and 90 K (LSCO), well above T_c and well below pseudogap temperatures (and presumably T_{mag}, which is likely to be especially large in YBCO because the chains facilitate vortex hopping).

From the "tilted hill" magnetic-field dependence that is observed both above and below T_c, the authors conclude[62,63] that the vortices are continuously present in the normal as well as in the superconductive state. This agrees perfectly with the present topological analysis, as does their observation that the vortices are inherently connected to pseudogaps. [In fact, the topological dielectric screening model is even stronger than their model. They assume that the energy for creating vortices in a magnetic field is smaller ("cheap") than in the homogeneous case (no pseudogaps), but at low temperatures, the dynamical loops in the present model are actually *native* to the self-organized dopant network (zero, or negative, formation energy).] The data present very serious difficulties for the many other theories they discuss, as those theories are all based on homogeneous mean-field lattice models without specific adaptive dopant configurations. These theories involve different kinds of additional assumptions (including rather far-fetched analogies with elementary particles and liquid crystals[67]), and they do not predict the dopant composition dependence, with its maximum near $x=(x_c+x_0)/2$. The presence of native diamagnetic loops also predicts field-enhanced diamagnetism, with composition dependence parallel to that of the Nernst effect, as observed.[63] Note that both vortex hopping and field loop enhancement assume that there is some "free area" available to vortex dynamics. This free area disappears as $x \rightarrow x_0$, where both effects become smaller.

If the B dopants are indeed in registry with the lattice, one can expect to find evidence in their structures for filamentary formation—provided that one is successful in searching the very large (~65 000 papers) cuprate literature. Several such recent examples have already been noted.[13] However, the most spectacular data found so far are in an old paper,[68] which reported data on the average kinetic energy $\langle E\rangle(T)$ of Cu ions in BSCCO measured by resonant neutron absorption spectroscopy; these are reproduced for the reader's convenience in Fig. 8. The results for optimally doped BSCCO ($\langle R\rangle=2.14$) show a steeper and more *linear* $\langle E\rangle(T)$ for high $T>T_0=145$ K than for undoped LCO ($\langle R\rangle=2.29$); as expected, the smaller $\langle R\rangle$ softens BSCCO and increases T_c. [This enhanced linearity is reminiscent of the linearity in the planar resistivity associated with the Ando II line (Fig. 4).] The linear behavior above T_0 can be explained in terms of lattice softening by dopant loops in ponds. These loops have three hierarchically ordered vibrational modes: radial in plane, angular in plane, and z-axis buckling out of plane. Presumably, the last buckling mode is the softest, and it accounts for the linear behavior above T_0. The stiffening below

T_0 arises as filamentary segments connect these loops. This is a perfect illustration of the zigzag (lateral and/or vertical) paths shown in Fig. 1. Incidentally, previous theories of precursive effects[62] contain no independent experimental evidence connecting T_0 to structure.

The great strength of this model is that it explains why the onset T_0 is about the same for the Nernst effect and Cu kinetic-energy arrest. This point could be tested conclusively by measuring $T_0(x)$, which is a very attractive experiment, especially considering that the experiments in Ref. 67 were done nearly 20 years ago and could easily be improved. The most interesting behavior, however, is the structural arrest between onset at T_0 and T_c This precursive effect becomes very steep near T_c, and it can be interpreted as a mean-field transition that "freezes" or merges filamentary end-loop connections. [The strain energy of a filamentary segment is harmonic and so is proportional to (the length) l^2; increasing the length by Δl increases the energy by $l\Delta l$, so that l itself is a mean field for filamentary end energies.] Note that the Meissner effect and the onset of superconductivity at T_c are easily explained in the filamentary model in terms of magnetic breakdown,[68] which reconnects filaments to form large diamagnetic loops. This rewiring is facilitated by lattice softening as described by $|\langle R\rangle - 2|^{-1}$.

XI. "HIGH-ENERGY" PSEUDOGAP

ARPES studies have revealed[69,70] that in addition to the $\sim$25 meV pseudogap seen in bulk properties (such as the resistivity, Figs. 3 and 4), there is an incoherent high-energy pseudogap between $E_1=0.4$ eV and $E_2=0.85$ eV in the one-electron spectrum. [As an aside, energies of order E_1, E_2 are "high" only in the context of the cuprates. In diatomic semiconductors such as GaAs, the $E(\mathbf{k})$ dispersion relations have been mapped out over an energy range up to 15 eV (Refs. 53 and 54) (the bulk plasma energy). One could even speculate that the onset of the incoherent high-energy range is related inversely to the complexity by the $\{(\text{number of atoms})/(\text{unit cell})\}^2$.] Nine examples were studied,[69,70] in an effort to establish chemical trends, including four samples of BSSCO (2212) ranging from under- to overdoped, with the optimally doped sample both above and below T_c. The broad trends were much the same, with small differences in anisotropies in momentum space, which are probably caused by host disorder (for instance, in PbBSCCO [where $R(\text{Pb})=2$, as in the perovskite $PbTiO_3$ compared to $R(\text{Bi})=3$] or BSCCO(2201) (stacking faults). In what follows, emphasis is placed on the data on BSCCO (2212) (which has the best ordered host lattice). Of course, this gap has nothing to do with spins, superexchange, antiferromagnetism, etc., on lattices. What causes it and how is it related to the pseudogap at the Fermi energy?

An example of the BSCCO (2212) data is shown in Fig. 3 of Ref. 70. Between $E_F=0$ and $E_1\sim 0.3$ eV, the energy distribution curves (EDCs) agree well with the momentum distribution curves (MDCs), as expected for normal quasiparticles. However, for $E>E_1$, the two curves bifurcate, with the EDCs flattening out at $E(k)\sim E_1(k_1)$ for $k>k_1$ and the MDCs becoming nearly vertical at $k=k_1$. It is important to realize that such a bifurcation cannot occur in mean-field theory, which always yields a single dispersion relation, except near level crossings. Also, note that these curves describe peak positions normalized above the elastic background [Fig. 2(a) of Ref. 69]. These positions depend on the way that the quasiparticle peaks are incoherently broadened by disorder, especially the disorder generated by dopants, as the mobile quasiparticle states of interest are filaments derived from dopant-centered orbitals. [The broadening of the nodal MDC is shown as an inset to Fig. 2(b) of Ref. 69.]

There have been many direct studies of near-infrared energy range 0.3–1.0 eV, including some on "ideal" (micaceous) Bi(2212), yet none of these studies have resolved incoherent anomalies. One obvious advantage of ARPES is that it is able to study separately EDCs and MDCs. Another, less obvious, advantage is that the optical matrix elements $\langle i|\mathbf{p}|f\rangle$ for photoexcitation to $\sim$20 eV are very sensitive to glassy disorder. The final states f near 20 eV are very nearly ideal Bloch states, as the dopant potentials perturb such high-energy states only weakly. Thus, the optical matrix element projects the amplitude and phase of the glassily disordered initial state i on a periodic state final state f, i.e., it samples the periodically coherent part of i in a phase-sensitive way. The same kind of phase coherence is involved in estimating the conductive contribution of a metallic filament to dielectric screening energies. It would be wrong to ignore the phase effects of disorder on the grounds that electron microscopy of cuprates shows apparently ideal lattices, or to attempt to calculate such effects solely from phase-insensitive Debye-Waller factors measured by diffraction. It would be even worse to attempt to describe the effects of disorder on complex orbital motion using a mean-field quasiparticle model. Worst of all would be a model restricting attention to the CuO_2 planes only and representing the disorder by fluctuations in fictive antiferromagnetic spins at the Cu lattice sites.

With this background, one can begin to interpret the main qualitative features of Fig. 3 of Ref. 70. By constraint counting,[1,12] or simply from the constancy of the planar lattice constant, it is clear that the only rigid and strongly periodic planes in the multiplanar cuprates are the isostatically rigid CuO_2 planes ($R=2.4$). So long as the optically weighted density of quasiparticle states is dominated by initial states i in this plane, there will be simple quasiparticles excitations, and there will be good agreement between the EDCs and MDCs. (The optical weighting varies with energy, and this is why the one-electron self-consistent field calculations of Ref. 55 are so successful.) However, for $E>E_1$, the CuO_2 planes no longer dominate the optically weighted density of quasiparticle states i; instead, other states become important, presumably the SrO semiconductive valence states, where the dopant interstitial O in BSCCO (for example) is thought to reside.[60] Unlike the isostatically rigid CuO_2 planes, the SrO layers are soft (or floppy, in the language of constraint theory[1,12]) with $R=2.0$, and so they are strongly disordered, both because of their native network instability and by the presence of coplanar off-lattice oxygen interstitial dopants. Thus, the leading effect is a reduction in quasiparticle peak amplitude, or the formation of an incoherent pseudogap for $E>E_1$. It is worth emphasizing that, unlike the pseudogap pinned to E_F, this "pseudogap" is not a gap in the density of quasiparticle states i but only in the optically weighted density of quasiparticle states i measured by heights and widths of peaks normalized above the elastic background.

What happens to the coherence (relative to that of the CuO_2 planes) of states i in the SrO planes? There will be a lot of relaxation around the dopant oxygen interstitials, especially near coplanar twofold coordinated host oxygens. We do not need to know the details of this relaxation, which is quite complex, even in the oxygen neighbors of substitutional Sr in LSCO as studied by EXAFS.[13,71] Our main goal is to understand the mechanism responsible for the bifurcated energy- and momentum-dispersion relations at E_1 and k_1 shown in the upper panel of Fig. 3 of Ref. 70. The overall angular picture is that in Bi(2212), the ARPES intensity integrated from 0 to 0.8 eV binding energy is largest in the antinodal (10) directions [Fig. 4(b) of Ref. 70], where electron-phonon interactions and both the superconductive and low-energy pseudogaps are the largest. This suggests that strongly coupled electron–LO-phonon interactions increase the coherence of the optical matrix elements; these same LO interactions are responsible for the shifts $\Delta\omega_{LO}$ shown here in Fig. 2(b). The quasiparticles formed by such coupled interactions are called polarons.

There is a large mathematical literature on polarons, but they are usually discussed in the context of simplifying approximations, such as translational invariance or one LO mode only. In the cuprate context, we have spatially inhomogeneous channels formed by nanodomains and layers with different strengths of LO-phonon–electron coupling, as well as dopant pinning of carriers. This means that it is not easy to apply polaron formalisms to the cuprates. Broadly speaking, there are two kinds of polarons; weakly coupled polarons are those similar to free carriers, but with small increases in effective mass, while strongly coupled carriers form bound-carrier–LO-phonon complexes, which give rise to self-trapping. Photoexcited carriers in the cuprates can form bound complexes, provided that sufficient phase space is available, and such complexes will lead to a crossover from coherent to incoherent ARPES distributions. In the low (binding) energy region, $E<E_1$, $|k-k_F|<|k_1-k_F|$, the effective wavelengths for localization are comparable to or larger than average channel widths. As E and $|k-k_F|$ increase, at a certain point $k=k_1$, it will become possible for bound complexes to form in channels. This energy $E(k_1)$ will scale with the bare bandwidth, in agreement with experiment.[72] A second factor that should contribute in forming bound complexes is the softening of the host lattice in the ($R=2$) SrO layers; as discussed above, increasing E increases the fraction of the quasiparticle density of states in these layers.

Kittel tabulates chemical trends of polaron coupling constants α (sometimes called λ) for the most studied diatomic ionic crystals (alkali and silver halides, where polarons are self-trapped) and a few partially ionic semiconductors.[73] In the former group, α ranges from 1.7 (AgBr) to 4.0 (KCl), while in ZnO ($\langle R\rangle=2$, a strongly ionic semiconductor, which is a borderline case) $\alpha=0.85$. SrO, which has the NaCl structure and also has $\langle R\rangle=2$, should have a larger value of α than ZnO, $\alpha(\mathrm{SrO})\sim 1$, and the local value at interstitial O should be much larger, comparable to the Ag halides. Thus, polaron self-trapping is expected for interstitial O in the SrO layers of the cuprates. When self-trapping occurs, there is a wide range of momenta for a given polaron energy. Thus, formation of bound polarons near O interstitials in the SrO layers explains semiquantitatively the flattening of the EDC's as E approaches E_1, as well as their angular dependence.

What about the MDCs, which show that in the SrO energy range between E_1 and E_2, the peak momentum $k=k_1$ is apparently constant (energy "waterfall")? This suggests the presence of a charge-density wave in the floppy SrO plane generated by the bound polarons and interstitial oxygens. This CDW is unrelated to the CDW associated with the pseudogap in the CuO_2 planes, in accordance with the experimental observation that the high-energy bifurcation is observed with similar strengths in all samples, including overdoped Bi(2212), where pseudogaps in the CuO_2 planes are much weaker than in underdoped Bi(2212). Moreover, although the presence of interstitial oxygens enhances the softening of the $R=2.0$ SrO planes relative to the isostatically rigid ($R=2.4$) CuO_2 planes, this effect is small, as the SrO planes are floppy anyway.[1,12]

The waterfall has also been studied[74] in optimally doped LSCO, with results that are qualitatively different from those obtained on the BSCCO family.[69,70] In LSCO, the Sr dopants are nearly substitutional, and the connectivity of the internal dopant network is determined by the large displacements of the oxygens that are first (10) and second (21) neighbors of the Sr dopants.[71] These displacements are strongly influenced by the host-lattice structure and the relative oxygen (10) and (21) weights. Thus, the self-trapping effects can be expected to exhibit some kind of d-wave anisotropy, as observed: a remarkable effect, and very pretty,[84] which is absent from BSCCO, where the oxygen interstitials are responsible for the waterfalls. Given that the (10) first-neighbor interactions must be much larger than the (21) second-neighbor interactions, the form of the d-wave anisotropy is explained, as well as its large magnitude $[E_1(\pi/4)\sim 10E_1(\sim 0)]$. The most surprising feature of these data is the small value of $E_1(\sim 0)$. It seems likely that the onset of decoherence at such low energies in LSCO (relative to the micaceous BSCCO results) is caused by surface roughening. The dopant dependence from $x\sim 0$ up to $x\sim 0.3$ of the largest $E_1(\pi/4)$ is nearly linear in x. This could well reflect a decrease in surface roughening as dopants are added, making the surface softer and less brittle.

XII. INFRARED PHASE DIAGRAMS

At this point, it is convenient to make a few more comments on infrared measurements.[58] Relative to ARPES experiments, the information contained in infrared data is limited by several factors (surface quality, exposure to air, and convolution of disordered initial with disordered final states). Thus, only the phase diagram of the unprocessed reflectivity is easily interpreted. It shows (Fig. 1 of Ref. 58) the largest change between 40 K and T_c at around 500 cm^{-1}, where R jumps from 0.95 to 0.98. Moreover, the (40 K, T_c) reflectivity change ΔR at optimal doping ($T_c=88$ K) is about three times the differences ΔR observed for slightly underdoped (T_c=66 K) and overdoped (T_c=77 and 67 K), even at 100 cm^{-1}.

The effects of inhomogeneities are quite striking: for the underdoped and overdoped samples, the (40 K, T_c) reflectivity changes increase slowly with decreasing frequency, but for the optimally doped sample almost all the change ΔR occurs virtually as a step function around 500 cm^{-1}. (In Ref. 74, this important point is not mentioned, as the discussion is focused on interpreting various features of optical functions derived from deconvolutions of reflectivity and ellipsometric data.) This abrupt appearance of an optical superconductive gap only at optimal doping shows that *at optical wavelengths*, the space-filling nature of the optimally doped filamentary network produces a sharp gap distribution, in strong contrast to the STM data,[5] which show a broad distribution of superconductive gaps at all doping levels at nanometer length scales.

The appearance of such homogeneity at a length scale 100 times larger than the nanodomain scale reflects the hierarchical nature of stress relaxation.[64,65] Probably, the simplest explanation for the large step function at optical doping is that only there is the earliest post-cleavage surface oxidation thin film uniform. (Long-term oxidation would probably produce a nearly insulating surface with little superconductivity.) This would also explain why such patchiness was not observed in selected areas of the STM virgin samples cleaved in vacuum *in situ*.[5] In any event, the disappearance of oxide patchiness at optimal doping is reminiscent of the disappearing isotope effect, also at optimal doping, discussed in the next section. Both effects reflect space filling by the filamentary network, with only the oxide patchiness being a surprising consequence of long-range stress fields: it reminds us of the delicate (possibly catalytic) nature of initial oxidation kinetics.

Note also that this optimally doped jump $\Delta R \sim 0.03$ is still present, but weaker ($\Delta R \sim 0.015$), in the reflectivity data for T=150 K and even T=220 K. The natural interpretation for this is that precursive superconductive pseudogaps—possibly associated with the dopant loops discussed in Sec. X (or merely filamentary fragments too short to generate a bulk Meissner effect)—are contributing a jump even well above T_c. How are these pseudogaps related to the pseudogaps identified in Figs. 3 and 4? To answer this question, we look at the unprocessed reflectivity data for the slightly underdoped (T_c=66 K) and overdoped (T_c=77 and 67 K) samples. All these samples exhibit a break in slope for the (40 K, T_c) curves compared to the (150 K, 220 K) curves around 1000 cm^{-1}. In the overdoped (T_c=77 and 67 K) samples, this corresponds to a negative curvature above 1000 cm^{-1}, which has been identified as a Fermi-liquid lifetime effect;[74] this is what our model predicts, as the Fermi-liquid patches can dominate the resistivity even below 1000 cm^{-1}, so long as T is above T_c. In the underdoped samples, the break in slope corresponds to a positive curvature, as the filamentary effects become much more pronounced below T_c. These precursive superconductive filamentary pseudogaps are different from the intraplanar interfacial pseudogaps illustrated in Fig. 1. The pseudogaps shown in Figs. 3 and 4 could well be influenced by both of these gaps.

It is instructive to compare the optical spectra of the cuprates to those of commercially available semiconductors, which have been analyzed in great detail;[53,54] high-quality semiconductor surfaces are easily prepared. The Kramers-Kronig procedures used in Ref. 74 to analyze cuprate spectra became standard in the context of semiconductor reflectivity measurements in the 1960s and 1970s for good reasons, namely, the random phase or one-electron approximation is valid for the semiconductors and the line shapes of interband thresholds, saddle points, etc., are best expressed in terms of $\varepsilon_2(\omega)$, the imaginary part of the dielectric constant, even when excitonic Coulomb interactions deform saddle-point edges.[53] For the ceramic oxides, however, it appears that the main features of the data are seen most clearly in the reflectivity itself.

XIII. ISOTOPE EFFECTS

The rich and impressive database established for the cuprates over the past 20 years has proven to be more than challenging for various theories, especially the exotic ones that insist that attractive electron-phonon interactions are not responsible for forming Cooper pairs.[37,75] There are 3 meV isotope effects in both ARPES dispersion relations[27,28] and inhomogeneous gaps measured by STM,[26] while recent improvements in ARPES resolution have even led to the identification of phonon fine structure in the nodal directions in LSCO (Ref. 76) similar to the Eliashberg fine structure occasionally seen much earlier in uncontrolled tunneling experiments.[77] However, even in conventional theories, many puzzles remain: for instance, why does the isotope effect in T_c become very weak as $T_c(x)$ approaches either a plateau or $T_c^{\max}$ Ref. 26? Some theorists have even argued that the disappearing isotope effect is a strong evidence for electron-spin, rather than electron-phonon interactions, as the cause of HTSCD.[6,75] Phenomenologically, we already know from the master curve for $T_c^{\max}$ [Fig. 2(a)] that the optimized isotope shift could be very small, as $\langle R\rangle$ is dimensionless; in any event, it can appear only in the scaling factor Θ and should be universal. Is there not a more detailed microscopic explanation?

Filamentary theory readily explains the disappearing T_c isotope effect as follows: in underdoped samples, where the isotope shifts are normal, T_c is determined by the Debye phonon energy scale θ_D or ω_D for electron-phonon interactions, just as in BCS theory.[7] However, as $T_c(x)$ approaches either a plateau or $T_c^{\max}$, the filamentary switching needed to form Meissner or Abrikosov (type II) perfectly diamagnetic loops becomes severely restricted: fluctuations in composition x or isotopic weight do not enhance T_c, because dT_c/dx is small. This space-filling explanation assumes that the larger zero-point vibrational amplitudes normally associated with larger ω_D and smaller masses are hindered by the space filling which has occurred as T approaches $T_c^{\max}$. With harmonic potentials increasing ω_D increases $\langle r^2\rangle$ (zero-point vibrations). Most of each filamentary path is planar, so increasing $\langle r^2\rangle$ is equivalent to increasing x: $T_c(x,\omega_D)=T_c(x/\omega_D)$. Alternatively, the vibrational amplitudes are larger, but this merely increases filamentary overlap, which increases the fraction of Fermi-liquid regions where $T_c=0$, thus off-setting the enhancement of T_c by the increase in the phonon energy scale ω_D on filaments. This is the same space-filling mechanism that causes dT_c/dx to go to zero, so the proportionality of the isotope shift and $d\log T_c/d\log x$ is expected, as a natural consequence of the existence of the Boolchand filamentary intermediate phase between the insulating and Fermi-liquid phases, or the reduction in free volume available for filamentary formation. Once one recognizes the failure of continuum models to describe space-filling aspects of off-lattice (glassy) percolation quantitatively, the "mystery"[6] of the vanishing isotope effect is solved.

The reader should note that the relation $T_c(x,\omega_D)=T_c(x/\omega_D)$ has not been derived using a power-series expansion, so it could, in principle, be exact. In practice, the dopant configuration is "frozen" at some temperature T_0 (similar to the vortex onset temperatures discussed in Sec. X), and so small corrections to this relation are possible. In practice, isotope exchange experiments are difficult, and it seems more likely that any observed discrepancies probably arise experimentally.

The fundamental contrast between lateral planar motion in the isostatic CuO_2 planes[1,12] and dopant-assisted vertical tunneling through ultrasoft semiconductive layers such as SrO is brought out by site-selective isotope experiments on T_c in YBCO.[26] There the results are quite surprising: the overall trends are described as above, but the cancellation at optimal doping is exact only for oxygen substitution at the soft and glassy apical oxygens or the CuO_x chains (low R sites). At the rigid and almost perfectly crystalline CuO_2 planes, there is a residual isotope shift even at optimal doping.

XIV. PARALLELS WITH NANOCRYSTALLINE TRANSITION-METAL OXIDE INTERFACES AND SUPERIONIC CONDUCTORS

The requirement of network self-consistency—especially with respect to internal stress—is very important, and it is responsible for the functional parallels between HTSC and network glasses shown in Fig. 2(a). However, to obtain more detailed electronic information, one should study simple systems that are closer to the cuprates, such as the nearly planar-lattice-constant-matched cubic perovksites $SrTiO_3$ and $LaAlO_3$ heterointerfaces[78] and thin-film nanocrystalline TiO_2, ZrO_2, and HfO_2.[79] There are many striking parallels between the results obtained both electrically and spectroscopically (probing both valence- and conduction-band energies separately) in these materials and in the cuprates. The most striking similarity is that with increasing grain size, electronic band coherence appears at a grain size of 3 nm, the same size as the average gap nanodomain seen in the cuprates by STM.[5] This validates the fundamental assumption of the filamentary percolative model, that the ideal metallic CuO_2 planes of the cuprates are, in fact, broken up into coherent 3 nm units separated by interfaces with pseudogaps (see Fig. 1, which dates from 1990). With regard to the existence of "invisible" filaments, one should note the theoretical work on Ag fast ion glassy solid electrolytes,[80] which, in the area of ionic transport, are just as spectacular as HTSC are for electronic transport. There the topological approach based on identifying filaments is very successful. The filaments are composed of structural units with free volumes $\mathcal{F}$ above average and are smoothly self-organized to minimize free volume differences $\delta\mathcal{F}$ between successive filamentary cells, which minimizes scattering due to density fluctuations. Large-scale numerical simulations then predict ionic conductivities over 11 orders of magnitude and show that the activation energy E_σ for ionic conduction (analogous to a pseudogap or superconductive gap energy) scales with $\mathcal{F}^{d/3}$ with $d=1$. Of course, none of these results are obtainable by analytic methods. Quite generally, over the past five years (since the discovery of the Boolchand intermediate phase in network glasses[1,21]), numerical simulations using a variety of methods have always reached the same conclusion that the Intermediate Phase is filamentary in nature.[52]

XV. CONCLUSIONS

Filamentary theory, based on topological reasoning, is well suited in discussing strongly disordered oxides such as the cuprates. These materials are all anomalously soft (elastically marginally stable, especially near dopants, with $\langle R\rangle < 2.4$ [Fig. 2(a)]). The remarkable cusped peak in $T_c^{\max}(\langle R\rangle)$ is shifted from the magic (stress-free) value $\langle R\rangle=2.40$ in network glasses to the electrically optimal supercritical value $\langle R\rangle=2.00$ in the cuprates. The marginal elastic stability of such anomalously soft (glassy or nearly glassy) oxides is quantitatively described by constraint theory, including the key role played by the CuO_2 planes. It is important to realize that the successful description of $T_c^{\max}$ with the resonating bond variable $\langle R\rangle$ [Fig. 2(a)] has far-reaching implications. Specifically, unless an alternative description can be found that relies on lattice periodicity and atomic coordination numbers (for instance, coordination number of 5 for Cu instead of the resonating bond number of 2), it will be impossible to describe cuprate HTSC with *any* nonpercolative lattice model. It will be interesting to see if anyone can find a configuration coordinate different from $\langle R\rangle$ that is equally effective in describing $T_c^{\max}$.

I tried average cation-anion Pauling electronegativity differences [which are the simplest measure of (currently popular) strong Coulomb interactions U], but this gave only scatter plots (as expected). Overall, $\langle R\rangle$ has proven itself to be a far more accurate guide to the properties of network glasses and strongly disordered crystals than it has in nearly ideal crystals or even small molecules, which means that strong disorder greatly enhances the value of $\langle R\rangle$ as a configuration coordinate.

Pictorially, the success of Fig. 2(a) requires that the structure seen by Cooper pairs at almost any given moment is one of the broken site symmetries in which each atom α has only $R(\alpha)$ nearest neighbors, and not the much larger number given by the time-averaged, largely dopant-independent symmetrically coordinated structure seen by diffraction or STM. Even at high temperatures, lattice models are deceptive, as there is always some dynamically broken local sym-

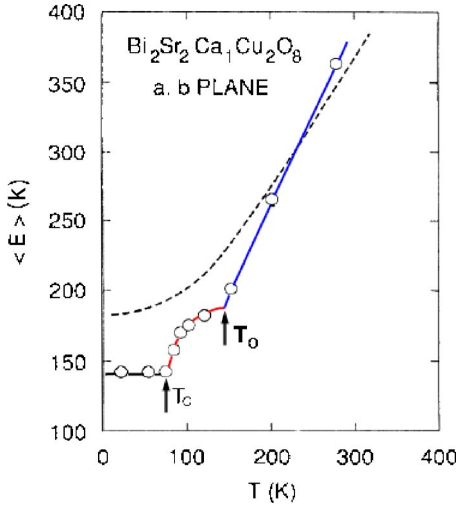

FIG. 9. (Color online) $\langle E \rangle (k)$ of Cu ions, redrawn from Ref. 68. The dashed line is a scaled calculation for a parent (undoped) compound, LCO. Note that doping linearizes and softens $\langle E \rangle (k)$ for $T > T_0 = 145$ K and introduces an abrupt stiffening for $T < T_0$, which then shows a "phase transition" as $T \rightarrow T_c$.

metry. As T decreases, these dynamically broken symmetries begin to condense around the electrically active B dopants, first forming the precursive dopant vortices (Sec. X and Fig. 9) and eventually forming the deformed B dopant networks that become superconductive. The condensation mechanism involves the instabilities of all the atoms [Fig. 2(a)] and, in fact, is mechanically stabilized (short of the Jahn-Teller distorted insulating phase), not promoted, by the CuO_2 planes, which are the relatively most rigid and locally symmetrical components of the network. These are the symmetries seen, for example, by STM (which cannot resolve distortions on a scale of 10^{-2} nm, especially as it averages over laboratory times, whereas the broken symmetries fluctuate on time scales shorter than microseconds).

In the absence of a lattice model, how do we proceed to analyze the rich experimental database? Chiefly, one makes use of the fact that the resonating bond network fills space efficiently. There are at least *five* space-filling features of the huge 65 000 paper HTSC database that are inexplicable with analytic models: the Ando II critical line (Fig. 4), the exciton relaxation time jump (Fig. 6), the reflectivity jump (Fig. 1 of Ref. 74), the near disappearance of the isotope effect, all occurring near optimal doping, and the chemical trends in the waterfall effect. Similar space-filling effects have been observed in many numerical simulations of the Boolchand intermediate phase.[52]

While the theory is far from complete, it is realistic because it takes into account the strongly disordered, off-lattice glassy character of doped cuprates, which is by now extremely well documented by STM experiments, especially those of Lang *et al.*[5] Lattice models are fixed, ignore this disorder, fail to explain $T_c^{\max}$, and generally are incapable of recognizing or explaining space-filling features, such as the discontinuities at optimal doping discussed in Sec. VIII. They cannot be expected to be anymore successful in describing the cuprates than spin-glass lattice models are in discussing the composition-dependent properties of real glasses such as window glass.[22] Moreover, plane-wave lattice models cannot consistently explain the observed d-wave anisotropy of the energy gap and the large magnitudes of T_c.[81] They predict a value of T_c of $YBCO_{6.5}$ (if all the O ions are fixed at ideal lattice sites) that is too small by a factor of ~ 100.[82] Strong disorder and space filling complicate the theory, but they also provide the flexibility and adaptability that make HTSC possible.[1]

ACKNOWLEDGMENTS

This paper benefited greatly from the presentations and discussions at the workshop http://cnls.lanl.gov/Conferences/latticeeffects/ sponsored by Los Alamos National Laboratory.

APPENDIX

There are spatial inhomogeneities in manganite perovskites [for instance, $(La,Ca)MnO_3$] with filamentary topologies similar to those in the cuprates. Recent large-scale two-dimensional Monte Carlo calculations use the traveling-cluster method to describe broken symmetry on an atomic scale.[83] These calculations show that, even with only short-range exchange interactions, near and above the metal-insulator transition, on-lattice polaronic carrier charge inhomogeneities also have a filamentary (not cluster, droplet, or "puddlelike") structure (similar to that found in classical models[52]), even though the carriers are not pinned to the (immobile Ca) dopants. This is presumably a bandwidth or kinetic-energy effect, as the toy Hamiltonian used in these calculations does not include long-range effects associated with Coulomb interactions and dynamical dielectric screening, which is the dominant force driving dopant ordering in the present model of the cuprates.

It is interesting to compare the filamentary patterns derived in the $(La,Ca)MnO_3$ simulation (their Fig. 3) with those derived by analyzing galactic cluster haloes (redshifts) (Fig. 11 of Ref. 84) generated by dark matter. The latter occur on very large length scales, yet their filamentary structure (the "cosmic web") is much more clumped (with larger voids separating the filaments) than that of the former. Most recent theoretical discussions of galactic clusters are carried out using hydrodynamic models somewhat similar to those used here in Sec. X: the voids in the cosmic web correspond to the ponds here. Three-dimensional mapping of dark matter has revealed a filamentary scaffold,[84] which could be caused by gravitational collapse. It could also be caused by a more complex balance of attractive and repulsive interactions similar to those involved in forming the HTSC filamentary network.

Fourier analysis of STM experiments on BSCCO has shown[85] that dopant (oxygen interstitials)-phonon coupling is very large in the normal state, and even larger in the superconductive state, as assumed here in Sec. VI to explain the evolution of ARPES Fermi arcs. The Fourier analysis does not include filamentary effects, which are necessary to understand the origin of the interactions they parametrize. On $YBa_2Cu_3O_{6+x}$, with $x \sim 0.35$, close to the metal-insulator transition, Ref. 86 reports thermal conductivity and electrical resistivity measurements that are inconsistent with continuum models. The samples are time doped, that is, although initially insulating, they develop metallic and superconductive properties by self-annealing. The obvious mechanism for such self-annealing is lowering of the free energy by filamentary formation to enhance dielectric screening.

The present model emphasizes modulations of the "soft" SrO layers, compared to the rigid CuO_2 planes. Recent studies of HTSC in two-phase samples of $Sr_2CuO_{3+\delta}$ ($\langle R\rangle=2.0$, see Fig. 2(a); the O_δ are on the apical sites of LSCO) provide strong support for the present model.[87] The authors were able to enhance T_c from 70 to 95 K by suitable purification and annealing below 300 °C (which does not change δ; in effect, the samples are self-annealed). Diffraction studies showed that this enhancement occurred in samples with modulated SrO layers, in excellent agreement with the present model (Fig. 1). The crystal symmetry of the 70 K phase is orthorhombic, while that of the 95 K phase is reduced to weakly monoclinic, as one would expect from a phase that is characterized by its dopant-centered curvilinear filamentary connectivity. These experiments dramatically illustrate the inadequacy of all theoretical lattice-based models, especially those based on mean-field approximations, and the importance of interlayer dopant-centered filamentary paths.

The authors of Ref. 87 ask "why does apical oxygen ordering have such a significant effect on T_c," but they are unable to answer this question within the framework of energy band (mean-field) theory. As an historical footnote, a survey of 273 papers (1994 to present) on "dopants +superconductivity" on the SCI indicates that only nine of these discuss percolation, while Ref. 88 discussed electrically active interlayer (apical) bistable dopants in a percolative context. By following the percolative trail starting from Ref. 88 the authors of Ref. 87 would have found the answer to their question, which is contained in the 20-yr-old Fig. 1 of this paper. In order for currents to flow beyond pseudogap barriers, they must use suitably placed interlayer bridges.

Quite recently,[89] $Ba_2Ca_3Cu_4O_8F_2$ (F0234) has been reported to be a high-temperature super conductor with $T_c=60$ K. This value falls on the master curve of Fig. 2(a) for $T_c^{\max}(\langle R\rangle)$, as shown there with this point added. This suggests that however complex its detailed electronic structure may be,[89] F0234 is still subject to the same optimization principles as all the other cuprates. With regard to the Lanzara waterfalls[70] discussed in Sec. XI, an explicit 4×4 checkerboard CDW model[90] describes the main features of the EDCs and MDCs of BSCCO.

Two-dimensional images do not resolve three-dimensional filaments, unless the latter can be reconstructed through a series of tomographic slices.[84] In the HTSC layered cuprates, this is not possible because STM looks only at the first few atomic layers. Moreover, the early surveys[5] tended to focus on nearly optimally doped samples, where separating pseudogaps from superconductive gaps is difficult. In strongly underdoped samples, the smaller superconductive gap Δ_s is well separated from larger pseudogaps Δ_p. There Ref. 91 reports the results of studying the difference between metallic and insulating (pseudogapped) surface regions through the weak (less than a factor of 2) tunneling ($\pm$) asymmetry of dI/dV in two cuprate samples, with $\langle R\rangle$ either greater than or less than 2. Strong rectifying I-V asymmetry occurs in semiconductor p-n junctions, but more generally it occurs whenever there are internal potential barriers, as in Coulomb blockade,[92] which, of course, is a larger effect in insulating (pseudogapped) regions. The STM scans reveal no connected metallic regions of the uppermost layers, which is unexpected, as the underdoped samples are still metallic and superconductive. Instead, there is a complex bilinear labyrinth of metallic filaments [small ($\pm$) asymmetry] in the upper CuO_2 plane that exhibit erratic and asymmetric superconductive gaps in dI/dV. These appear to be interrupted by a second bilinear array of crossing semiconductive filaments [large ($\pm$) asymmetry], where the superconductive gap structure is still visible (proximity effect) but is statistically weaker.

According to Fig. 1 here, the metallic filaments are actually connected through hidden dopant bridges to lower CuO_2 planes; thus, in the upper CuO_2 plane, one *expects* to observe only filamentary segments. These segments strongly prefer to be linear, because (1) the antiferroelectric LO phonon (the half-breathing mode) softening is concentrated near the $(\pi,0)$ zone boundary, (2) this minimizes the kinetic energy of the metallic channel, and (3) the linear segments dielectrically screen larger adjacent areas (Sec. X). Disconnected linear metallic segments dominate observed STM patterns (Fig. 3 of Ref. 91) in both underdoped (but still superconductive) $Bi_2Sr_2CaCu_2O_{8+x}$ ($T_c=45$ K, $t=T_c/T_c^{\max}=0.5$) and $Na_xCa_{2-x-y}CuO_2Cl_2$ ($T_c=21$ K, $t=0.6$). The metallic segments are noticeably (Fig. 4 of Ref. 91) longer (more strongly self-organized) in the latter (softer, $\langle R\rangle<2$) than in the former (more rigid, $\langle R\rangle>2$); clearly, $\langle R\rangle$ is a much more useful configuration coordinate than t. Previously, ARPES experiments showed that the Fermi areas of NCCOC are too small to be consistent with mean-field band theory.[46] It is possible that the $p(x,y)$ O and Cl valence bands in NCCOC do not hybridize, as the O and Cl ions lie in xy planes separated by Na_xCa_{2-x-y} ions (including vacancies). Thus, Na and even Ca vacancies can function as interlayer dopants connecting CuO_2 planes, and pairs of dopants may be needed to form bridges across the Cl planes.

The dI/dV superconductive and pseudogap structures are reported for 72 dI/dV atomic characteristics in Fig. 5(B) of Ref. 91, but the statistical correlations of Δ_p asymmetry with Δ_s asymmetry are not yet available. In spite of proximity effects, the overall (±150 mV) dI/dV asymmetry distinguishes metallic from semiconductive filaments in both materials, because 150 mV is well outside the gap structures. Equally noticeable is that in BSCCO ($\langle R\rangle>2$), but not in NCCOC ($\langle R\rangle<2$), the Δ_p peaks are much stronger (weaker scattering) at positive energies ["conduction-band" peaks] than at negative ("valence band") energies; this feature is much larger than the Cu/O alternation stressed in Ref. 91. This is what one would expect, as in semiconductors where valence-band states are more localized than conduction-band states,[92] which gives rise to larger dopant-induced strain broadening of Δ_p at negative energies. This effect is reduced in more ionic insulators such as NCCOC ($\langle R\rangle<2$), where the Δ_p structure is much broader. [Specifically, there are many antiferroelectric phases[30] in oxide perovskites ($\langle R\rangle = 2.40$), but none in halide perovskites ($\langle R\rangle = 1.20$), which means that the presence of $R=1$ Na and Cl ions strongly scatters soft zone-boundary (antiferroelectric symmetry) modes that generate Jahn-Teller pseudogaps.]

For the 72 dI/dV atomic characteristics shown, the Δ_s correlations in both BSCCO and NCCOC are erratic. This is expected in the present strong disorder model, as the strongly attractive electron-phonon Cooper pairing interactions are localized at the negative U dopants that lie hidden between the CuO_2 planes. One can expect complex interference effects at surface atomic sites between Cooper pairs interacting with these distant buried dopants. The Cooper pairs form standing waves (antinodal at the dopants) and propagate along filamentary channels with $2k_F$ wave numbers, a natural generalization of Landauer wavelet interference in ballistic quantum channels.[93]

The superconductive gap itself equally mixes electrons and holes (Cooper pairs are neutral) and so should not be affected to first order in Δ_s/Δ_p by Coulomb blockade at dopants. However, the Δ_s voltages [$\sim$20(10) meV for BSCCO (NCCOC)] are easily large enough to induce a second-order rectifying effect in dI/dV through Coulomb blockade charge-density oscillations at the dopants similar to those seen in quantum dots.[94] These can alter electron-phonon interactions at the interlayer negative U dopants, which, in turn, affects the (±) tunneling asymmetry of local superconductive gaps measured at the surface atoms. (Dopant pairs function as source and drain contacts, while the STM probe is a gate.) Finally, in spite of fuzzing by proximity effects, the $2k_F$ periodicity of Δ_s should be recognizable as longer periodicities in NCCOC (small Fermi number, see Refs. 45 and 46) than in BSCCO (large Fermi wave number). This appears to be the case [compare rows 3 and 4 of Figs. 4(B), 4(E), and 5(B) of Ref. 91].

More generally, the fractal dimensionality d_s^* of the metallic superconductive channels can be estimated from the strength of the oscillations in Δ_s caused by nearest-neighbor dopants. These oscillations should scale with $N^{-1/2}$, where $N=2d_s^*$. The observed Δ_s oscillations in BSCCO are very strong, which suggests that $d_s^*=1$ (filaments). This appears to be a universal interference effect in each metallic one-dimensional channel; although it is very simple, this effect apparently is a *very strong* direct evidence for the filamentary paths (quantum percolation along ballistic channels) shown in Fig. 1 (from 1990).

Similar couplings also affect the Jahn-Teller pseudogaps, but the coupling constants in the two cases are different for many reasons (including the large voltage differences, as well as different plaquette pair scattering diagrams), so that the magnitudes of the two asymmetries are largely independent; this could also reflect the presence of two kinds of dopant sites (A, Δ_p, and B, Δ_s). This is why the (±) tunneling asymmetry of the low-energy 10–20 mV Δ_s structure does not match the (±) tunneling asymmetry Δ_p ($\sim$100+ meV) background on an atom-by-atom basis. The larger pseudogap amplitudes Δ_p in BSCCO suggest that there larger values of N are involved (in view of the observed 4×4 superstructure, probably out to at least second neighbors) and that $d_p^*=2-3$.

Reference 91 cautiously describes the observed structure as planar "electronic glass clusters." However, at low densities, such "clusters" or "droplets" are, in general, disconnected (localized or isolated, as in spin glasses, and the cuprate μSR studies cited in Ref. 91, or a very wide variety of nanoscopically inhomogeneous systems, for instance, polymers, colloids, sol-gels, metallic glasses, as well as the present underdoped cuprate planes). When *random* electronic clusters do merge at higher densities (as they would in the cuprate planes near optimal doping, $x=x_0$), a Fermi liquid is formed, and the phase diagram exhibits only one metal-insulator transition with no intermediate phase. [A good example is the nonmagnetic cubic perovskite $Ba_{1-x}K_xBiO_3$ (BKBO), where $T_c(x)$ is far from parabolic: instead, in overdoped samples, $T_c(x)$ increases steeply with decreasing x, reaching a maximum T_c of 34 K just at the single metal-insulator transition $x=x_0$, where dielectric screening of the electron-phonon interaction is minimal.[95]]

Experiments on other network molecular phase transitions and many classical numerical simulations have shown that merging *randomly* (phase incoherent) distributed clusters does not produce an intermediate phase; this is a fundamental and unavoidable point of theory that is essential for understanding HTSC.[1,52] The linear (one-dimensional) metallic segments observed experimentally in underdoped HTSC cuprates[91] are very strongly suggestive of the partially masked, zigzag, *phase coherent*, filamentary morphology connected around pseudogap barriers by the hidden interlayer bridges shown in Fig. 1.[14] It is just this self-organized lateral and/or vertical zigzag filamentary morphology that is responsible for the formation of the intermediate phase and HTSC,[1] partially resolved in Ref. 91. So far, the larger-scale channels sketched in Figs. 7 and 9 have not been observed by low-T STM, but they may become observable in high-T STM studies of underdoped samples.[34]

---

[1] J. C. Phillips, Phys. Rev. Lett. **88**, 216401 (2002); Philos. Mag. B **79**, 527 (1999); P. Boolchand, G. Lucovsky, J. C. Phillips, and M. F. Thorpe, Philos. Mag. **85**, 3823 (2005); for similar ongoing hydrodynamic debates, see G. Trevino and E. L. Andreas, Phys. Today **59** (11), 17 (2006); the dynamics of percolative formation of filaments is well described by J. C. Conrad, P. P. Dhillon, E. R. Weeks, D. R. Reichman, and D. A. Weitz, Phys. Rev. Lett. **97**, 265701 (2006).

[2] H. J. Choi, M. L. Cohen, and S. G. Louie, Phys. Rev. B **73**, 104520 (2006); J. E. Moussa and M. L. Cohen, *ibid.* **74**, 094520 (2006); P. Zhang, S. G. Louie, and M. L. Cohen, Phys. Rev. Lett. **98**, 067005 (2007).

[3] C. Renner, B. Revaz, J.-Y. Genoud, K. Kadowaki, and Ø. Fischer, Phys. Rev. Lett. **80**, 149 (1998).

[4] T. Cren, D. Roditchev, W. Sacks, J. Klein, J.-B. Moussy, C. Deville-Cavellin, and M. Laguës, Phys. Rev. Lett. **84**, 147 (2000).

[5] K. M. Lang, V. Madhavan, J. E. Hoffman, E. W. Hudson, H. Eisaki, S. Uchida, and J. C. Davis, Nature (London) **415**, 412 (2002); J. Jung, Physica C **364**, 216 (2001); J. Jung and J. C. Phillips, Philos. Mag. B **81**, 745 (2001).

[6] J. A. Wilson, J. Phys.: Condens. Matter **18**, R69 (2006).

[7] J. R. Schrieffer, *Theory of Superconductivity* (Perseus Books, Reading, MA, 1999).

[8] C. C. Tsuei, J. R. Kirtley, Jr., C. C. Chi, L. S. Yujhanes, A. Gupta, T. Shaw, J. Z. Sun, and M. B. Ketchen, Phys. Rev. Lett. **73**, 593 (1994).

[9] Z.-X. Shen, D. S. Dessau, B. O. Wells, D. M. King, W. E. Spicer, A. J. Arko, D. Marshall, L. W. Lombardo, A. Kapitulnik, P. Dickinson, S. Doniach, J. DiCarlo, T. Loeser, and C. H. Park, Phys. Rev. Lett. **70**, 1553 (1993).

[10] K. McElroy, R. W. Simmonds, D.-H. Lee, J. Orenstein, H. Eisaki, S. Uchida, and J. C. Davis, Nature (London) **422**, 592 (2003).

[11] K. A. Mueller, Philos. Mag. Lett. **82**, 279 (2002).

[12] J. C. Phillips, Philos. Mag. **85**, 931 (2005).

[13] J. C. Phillips, A. Saxena, and A. R. Bishop, Rep. Prog. Phys. **66**, 2111 (2003).

[14] J. C. Phillips, Phys. Rev. B **41**, 8968 (1990); Philos. Mag. B **81**, 35 (2001); **82**, 1163 (2002); Phys. Rev. B **71**, 184505 (2005); Philos. Mag. **83**, 3255 (2003); **83**, 3267 (2003).

[15] M. H. Cohen, L. M. Falicov, and J. C. Phillips, Phys. Rev. Lett. **8**, 316 (1962).

[16] Y. J. Uemura, Phys. Rev. Lett. **62**, 2317 (1989); Solid State Commun. **126**, 23 (2003).

[17] P. Böni, J. D. Axe, G. Shirane, R. J. Birgeneau, D. R. Gabbe, H. P. Jenssen, M. A. Kastner, C. J. Peters, P. J. Picone, and T. R. Thurston, Phys. Rev. B **38**, 185 (1988).

[18] J. C. Phillips, *Physics of High-T_c Superconductivity* (Academic, Boston, 1989).

[19] K. P. Bohnen, R. Heid, and M. Krauss, Europhys. Lett. **64**, 104 (2003).

[20] G. Van Tendeloo, O. I. Lebedev, M. Hervieu, and B. Raveau, Rep. Prog. Phys. **67**, 1315 (2004).

[21] S. Chakravarty, D. G. Georgiev, P. Boolchand, and M. Micoulaut, J. Phys.: Condens. Matter **17**, L1 (2005); C. Popov, S. Boycheva, P. Petkov, Y. Nedeva, B. Monchev, and S. Parvanov, Thin Solid Films **496**, 718 (2006).

[22] R. Kerner and J. C. Phillips, Solid State Commun. **117**, 47 (2001).

[23] T. Hanaguri, C. Lupien, Y. Kohsaka, D.-H. Lee, M. Azuma, M. Takano, H. Takagi, and J. C. Davis, Nature (London) **430**, 1001 (2004).

[24] I. Yamada, A. A. Belik, M. Azuma, S. Harjo, T. Kamiyama, Y. Shimakawa, and M. Takano, Phys. Rev. B **72**, 224503 (2005).

[25] O. Rosch, O. Gunnarsson, X. J. Zhou, T. Yoshida, T. Sasagawa, A. Fujimori, Z. Hussain, X. Z. Shen, and S. Uchida, Phys. Rev. Lett. **95**, 227002 (2005).

[26] H. Keller, Struct. Bonding (Berlin) **114**, 143 (2005).

[27] J. Lee, K. Fujita, K. McElroy, J. A. Slezak, M. Wang, Y. Aiura, H. Bando, M. Ishikado, T. Masui, J.-X. Zhu, A. V. Balatsky, H. Eisaki, S. Uchida, and J. C. Davis, Nature (London) **442**, 546 (2006).

[28] J. F. Douglas, H. Iwasawa, Z. Sun, A. V. Fedorov, M. Ishikado, T. Saitoh, H. Eisaki, H. Bando, T. Iwase, A. Ino, M. Arita, K. Shimada, H. Namatame, M. Taniguchi, T. Masui, S. Tajima, K. Fujita, S. Uchida, Y. Aiura, and D. S. Dessau, Nature (London) **446**, E5 (2007); H. Iwasawa, Y. Aiura, H. Eisaki, A. Ino, H. Namatame, and M. Taniguchi (unpublished).

[29] H. Uchiyama, A. Q. R. Baron, S. Tsutsui, Y. Tanaka, W.-Z. Hu, A. Yamamoto, S. Tajima, and Y. Endoh, Phys. Rev. Lett. **92**, 197005 (2004); D. Reznik, L. Pintschovius, M. Ito, S. Iikubo, M. Sato, H. Goka, M. Fujita, K. Yamada, G. D. Gu, and J. M. Tranquada, Nature (London) **440**, 1170 (2006); Y. Petrov, T. Egami, R. J. McQueeney, M. Yethiraj, H. A. Mook, and F. Dogan, arXiv:cond-mat/0003414 (unpublished).

[30] G. A. Geguzina, Integr. Ferroelectr. **64**, 61 (2004).

[31] J. C. Phillips, Phys. Status Solidi B **242**, 51 (2005).

[32] J. C. Phillips, Proc. Natl. Acad. Sci. U.S.A. **94**, 12771 (1997); **95**, 7264 (1998); D. Reznik, L. Pintschovius, M. Fujita, K. Yamada, G. D. Gu and J. M. Tranquada, arXiv:cond-mat/0611079, J. Low Temp. Phys. (to be published).

[33] K. McElroy, J. Lee, J. A. Slezak, D.-H. Lee, H. Eisaki, S. Uchida, and J. C. Davis, Science **309**, 1048 (2005); Y. He, T. S. Nunner, P. J. Hirschfeld, and H.-P. Cheng, Phys. Rev. Lett. **96**, 197002 (2006).

[34] A. Pasupathy, A. Pushp, K. Gomes, S. Ono, Y. Abe, Y. Ando, H. Eisaki, K. H. Kim, H. K. Lee, S.-I. Lee, and A. Yazdani, Bull. Am. Phys. Soc. **51**, 213 (2006).

[35] L. Pintschovius, Phys. Status Solidi B **242**, 30 (2005); D. J. Singh and W. E. Pickett, Phys. Rev. Lett. **73**, 476 (1994).

[36] D. Pavuna, J. Supercond. **13**, 867 (2000).

[37] P. A. Lee, N. Nagaosa, and X. G. Wen, Rev. Mod. Phys. **78**, 17 (2006).

[38] W. S. Lee, S. Johnston, T. P. Devereaux, and Z. X. Shen, Phys. Rev. B (to be published); arXiv:cond-mat/07040093 (unpublished).

[39] M. S. Osofsky, R. J. Soulen, J. H. Claasen, G. Trotter, H. Kim, and J. S. Horwitz, Phys. Rev. Lett. **87**, 197004 (2001); G. E. Tsydynzhapov, A. F. Shevchun, M. R. Trunin, V. N. Zverev, D. V. Shovkun, N. V. Barkovskiy, and L. A. Klinkova, JETP Lett. **83**, 405 (2006).

[40] Y. Ando, S. Komiya, K. Segawa, S. Ono, and Y. Kurita, Phys. Rev. Lett. **93**, 267001 (2004).

[41] H. He and M. F. Thorpe, Phys. Rev. Lett. **54**, 2107 (1985).

[42] J. Rohler, Physica C **408**, 458 (2004).

[43] H. Maeta, F. Ono, C. Kawabata, and N. L. Saini, J. Phys. Chem. Solids **65**, 1445 (2004).

[44] N. L. Saini and H. Oyanagi, Physica C **412**, 152 (2004).

[45] T. Yoshida, X. J. Zhou, T. Sasagawa, W. L.. Yang, P. V. Bogdanov, A. Lanzara, Z. Hussain, T. Mizoka, T. Fujimori, H. Eisaki, Z. X. Shen, T. Kakeshita, and S. Uchida, Phys. Rev. Lett. **91**, 027001 (2003); T. Yoshida, X. J. Zhou, K. Tanaka, W. L. Yang, Z. Hussain, Z. X. Shen, A. Fujimori, S. Sahrakorpi, M. Lindroos, R. S. Markiewicz, A. Bansil, S. Komiya, Y. Ando, H. Eisaki, T. Kakeshita, and S. Uchida, Phys. Rev. B **74**, 224510 (2006).

[46] K. M. Shen, F. Ronning, D. H. Lu, W. S. Lee, N. J. C. Ingle, W. Meevasana, F. Baumberger, A. Damascelli, N. P. Armitage, L. L. Miller, Y. Kohsaka, M. Azuma, M. Takano, H. Takagi, and Z.-X. Shen, Phys. Rev. Lett. **93**, 267002 (1994).

[47] A. J. Leggett, Nat. Phys. **2**, 134 (2006).

[48] M. Mayr, G. Alvarez, A. Moreo, and E. Dagotto, Phys. Rev. B **73**, 014509 (2006).

[49] D. Senechal, P. L. Lavertu, M. A. Marois, and A. M. S. Tremblay,

Phys. Rev. Lett. **94**, 156404 (2005).

[50] R. S. Markiewicz, Phys. Rev. B **70**, 174518 (2004).

[51] A. V. Chubukov and M. R. Norman, Phys. Rev. B **70**, 174505 (2004).

[52] C. Reichhardt, C. J. O. Reichhardt, I. Martin, and A. R. Bishop, Phys. Rev. Lett. **90**, 026401 (2003); E. Kaneshita, I. Martin, and A. R. Bishop, J. Phys. Soc. Jpn. **73**, 3223 (2004); J. Barre, A. R. Bishop, T. Lookman, and A. Saxena, Phys. Rev. Lett. **94**, 208701 (2005); C. Reichhardt, C. J. O. Reichhardt, and A. R. Bishop, Europhys. Lett. **72**, 444 (2005); P. S. Salmon, J. Phys.: Condens. Matter **18**, 11443 (2006); J. C. Phillips, Philos. Mag. B **81**, 757 (2001); M. V. Chubynsky, M.-A. Briere, and N. Mousseau, Phys. Rev. E **74**, 016116 (2006).

[53] J. C. Phillips, Solid State Phys. **18**, 56 (1966).

[54] M. L. Cohen and J. R. Chelikowsky, *Electronic Structure and Optical Properties of Semiconductors*, Springer Series on Solid State Sciences Vol. 75 (Springer, New York, 1988).

[55] S. Sahrakorpi, M. Lindroos, and A. Bansil, J. Phys. Chem. Solids **67**, 208 (2006).

[56] J. C. Phillips, Rep. Prog. Phys. **59**, 1133 (1996).

[57] N. Gedik, M. Langer, J. Orenstein, S. Ono, Y. Abe, and Y. Ando, Phys. Rev. Lett. **95**, 117005 (2005).

[58] F. Carbone, A. B. Kuzmenko, H. J. A. Molegraaf, E. van Heumen, V. Lukovac, F. Marsiglio, D. van der Marel, K. Haule, G. Kotliar, H. Berger, S. Courjault, P. H. Kes and M. Li, Phys. Rev. B **74**, 064510 (2006); J. C. Phillips, arXiv:cond-mat/0605217 (unpublished).

[59] K. McElroy, J. Lee, J. A. Slezak, D.-H. Lee, H. Eisaki, S. Uchida, and J. C. Davis, Science **309**, 1048 (2005).

[60] P. Richard, Z.-H. Pan, M. Neupane, A. V. Fedorov, T. Valla, P. D. Johnson, G. D. Gu, W. Ku, Z. Wang, and H. Ding, Phys. Rev. B **74**, 094512 (2006).

[61] A. Pasupathy, A. Pushp, K. Gomes, S. Ono, Y. Abe, Y. Ando, H. Eisaki, K. H. Kim, H. K. Lee, S.-I. Lee, and A. Yazdani, Bull. Am. Phys. Soc. **51**, 213 (2006); S. Zhou, H. Ding, and Z. Wang, Phys. Rev. Lett. **98**, 076401 (2007).

[62] Y. Wang, L. Li, and N. P. Ong, Phys. Rev. B **73**, 024510 (2006).

[63] Y. Y. Wang, L. Li, M. J. Naughton, G. D. Gu, S. Uchida, and N. P. Ong, Phys. Rev. Lett. **95**, 247002 (2005).

[64] K. H. Ahn, T. Lookman, A. Saxena, and A. R. Bishop, Phys. Rev. B **68**, 092101 (2003).

[65] D. J. Jacobs and M. F. Thorpe, Phys. Rev. Lett. **75**, 4051 (1995).

[66] B. Fauque, Y. Sidis, V. Hinkov, S. Pailhes, C. T. Lin, X. Chaud, and P. Bourges, Phys. Rev. Lett. **96**, 197001 (2006).

[67] D. D. Joseph, Proc. Natl. Acad. Sci. U.S.A. **103**, 14272 (2006).

[68] H. A. Mook, M. Mostoller, J. A. Harvey, N. W. Hill, B. C. Chakoumakos, and B. C. Sales, Phys. Rev. Lett. **65**, 2712 (1990); V. M. Gvozdikov, Phys. Rev. B **72**, 075135 (2005).

[69] J. Graf, G.-H. Gweon, K. McElroy, S. Y. Zhou, C. Jozwiak, E. Rotenberg, A. Bill, T. Sasagawa, H. Eisaki, S. Uchida, H. Takagi, D.-H. Lee, and A. Lanzara, Phys. Rev. Lett. **98**, 067004 (2007).

[70] J. Graf, G.-H. Gweon, and A. Lanzara, arXiv:cond-mat/0610313, Proceedings of the M2S-HTS, (to be published).

[71] D. Haskel, E. A. Stern, F. Dogan, and A. R. Moodenbaugh, J. Synchrotron Radiat. **8**, 186 (2001).

[72] Z.-H. Pan, P. Richard, A. V. Fedorov, T. Kondo, T. Takeuchi, S. L. Li, P. Dai, G. D. Gu, W. Ku, Z. Wang, and H. Ding, arXiv:cond-mat/0610442 (unpublished).

[73] C. Kittel, *Introduction to Solid State Physics* (Wiley, New York, 1986), p. 282.

[74] J.-X. Zhu, K. McElroy, J. Lee, T. P. Devereaux, Q. Si, J. C. Davis, and A. V. Balatsky, Phys. Rev. Lett. **97**, 177001 (2006).

[75] P. W. Anderson, P. A. Lee, M. Randeria, T. M. Rice, N. Trevedi, and F. C. Zhang, J. Phys.: Condens. Matter **16**, R755 (2004).

[76] X. J. Zhou, J. Shi, T. Yoshida *et al.*, Phys. Rev. Lett. **95**, 117001 (2005).

[77] D. Shimada, N. Tsuda, U. Paltzer, and F. W. de Wette, Physica C **298**, 195 (1998); G.-M. Zhao, arXiv:cond-mat/0610386 (unpublished).

[78] G. Koster, T. H. Geballe, W. Siemons, G. Lucovsky, H. Seo, J. Luening, and M. Beasley (unpublished).

[79] G. Lucovsky, L. B. Fleming, M. D. Ulrich, G. Bersuker, P. Lysaght, and J. Luening (unpublished).

[80] St. Adams and J. Swenson, Phys. Rev. Lett. **81**, 4144 (2000).

[81] D. M. Tang, J. Li, and C. D. Gong, Solid State Commun. **133**, 259 (2005).

[82] K. P. Bohnen, R. Heid, and M. Krauss, Europhys. Lett. **64**, 104 (2003).

[83] S. Kumar, A. P. Kampf, and P. Majumdar, Phys. Rev. Lett. **97**, 176403 (2006).

[84] J. M. Colberg, Mon. Not. R. Astron. Soc. **375**, 337 (2007); B. Schwarzschild, Phys. Today **60** (3), 20 (2007).

[85] J. Chang, S. Pailhes, M. Shi, M. Maansson, T. Claesson, O. Tjernberg, J. Voigt, V. Perez-Dieste, L. Patthey, N. Momono, M. Oda, M. Ido, A. Schnyder, C. Mudry, and J. Mesot, arXiv:cond-mat/0610880 (unpublished).

[86] N. Doiron-Leyraud, M. Sutherland, S. Y. Li, L. Taillefer, R. Liang, D. A. Bonn, and W. N. Hardy, Phys. Rev. Lett. **97**, 207001 (2006).

[87] Q. Q. Liu, H. Yang, X. M. Qin, Y. Yu, L. X. Yang, F. Y. Li, R. C. Yu, C. Q. Jin, and S. Uchida, arXiv:cond-mat/0611439 (unpublished); I. Bozovic, G. Logvenov, M. A. J. Verhoeven, P. Caputo, E. Goldobin, and M. R. Beasley, Phys. Rev. Lett. **93**, 157002 (2004).

[88] J. C. Phillips, Physica C **221**, 327 (1994); **252**, 188 (1995).

[89] Y. Chen, A. Iyo, W. Yang, X. Zhou, D. Lu, H. Eisaki, T. P. Devereaux, Z. Hussain, and Z.-X. Shen, Phys. Rev. Lett. **97**, 236401 (2006); W. Xie, O. Jepsen, O. K. Andersen, Y. Chen, and Z. X. Chen, *ibid.* **98**, 047001 (2007).

[90] T. Zhou and Z. D. Wang, arXiv:cond-mat/0612424 (unpublished).

[91] Y. Kohsaka, C. Taylor, K. Fujita, A. Schmidt, C. Lupien, T. Hanaguri, M. Azuma, M. Takano, H. Eisaki, H. Takagi, S. Uchida, and J. C. Davis, Science **315**, 1380 (2007).

[92] J. P. Walter and M. L. Cohen, Phys. Rev. B **4**, 1877 (1971).

[93] G. Kirczenow, Phys. Rev. B **39**, 10452 (1989).

[94] S. Datta, Nanotechnology **15**, S433 (2004).

[95] B. A. Baumert, J. Supercond. **8**, 175 (1995); G. E. Tsydynzhapov, A. F. Shevchun, M. R. Trunin, V. N. Zverev, D. V. Shovkun, N. V. Barkovskiy, and L. A. Klinkova, JETP Lett. **83**, 405 (2006).